12-2008

New Consolidation of Emission and Processing for Air Quality Modeling Assessment in Asia

Yuan Du
University of Tennessee - Knoxville

To the Graduate Council:

I am submitting herewith a thesis written by Yuan Du entitled "New Consolidation of Emission and Processing for Air Quality Modeling Assessment in Asia." I have examined the final electronic copy of this thesis for form and content and recommend that it be accepted in partial fulfillment of the requirements for the degree of Master of Science, with a major in Civil Engineering.

Joshua Fu, Major Professor

We have read this thesis and recommend its acceptance:

Wayne Davis, Terry Miller

Accepted for the Council:
Carolyn R. Hodges

Vice Provost and Dean of the Graduate School

(Original signatures are on file with official student records.)

To the Graduate Council:

I am submitting herewith a thesis written by Yuan Du entitled "New Consolidation of Emission and Processing for Air Quality Modeling Assessment in Asia". I have examined the final electronic copy of this thesis for form and content and recommend that it be accepted in partial fulfillment of the requirements for the degree of Master of Science, with a major in Civil Engineering.

Joshua Fu, Major Professor

We have read this thesis
and recommend its acceptance:

Wayne Davis

Terry Miller

Accepted for the Council:

Carolyn R. Hodges, Vice Provost and
Dean of the Graduate School

New Consolidation of Emission and Processing for Air Quality Modeling Assessment in Asia

A Thesis Presented for
the Master of Science
Degree
The University of Tennessee, Knoxville

Yuan Du
December 2008

ACKNOWLEDGEMENTS

I would like to express profound gratitude to my advisor, Dr. Joshua Fu, for his invaluable support, encouragement, supervision and suggestions throughout this research. His moral support and continuous guidance enabled me to complete my work successfully. I am also highly thankful to Dr. Wayne Davis and Dr. Terry Miller who are willing to serve as my committee and guide my study. Moreover, my sincere thanks go to Yun Fat Lam, Yunhee Kim and GaoYang for their kind help and valuable suggestions. I also wish to express my appreciation to Ms. Jennifer Spirko who helped me overcome my doubts in doing this thesis. Finally, I am as ever, especially indebted to my parents, Xing'an Du and Shizhou Han, who will be always there supporting me for my entire life.

ABSTRACT

Gridded Asian emission input with fine resolutions for regional photochemical air quality modeling is absent from current studies. A new top-down emission process based on GIS-FORTRAN program has been developed in this study to consolidate the current available regional emissions in Asia and provide model-ready emission input with more flexibility. The INTEX-B anthropogenic emission inventory in 2006 integrated with biogenic from GEIA, as well as biomass burning and ship emissions from TRACE-P has been adopted as the top-level emissions, which are then spatially allocated into grid-cell level by our GIS application. The spatial allocation factors generated for this process are mainly based on the latest geographic and socio-economic information from LandScan population, updated road network, and landcover from USGS. A chemical species mapping process has been applied to ensure all VOC emission are in CB05 species converted from TRACE-P species. The vertical assignment and temporal allocation are also implemented to obtain gridded hourly emission data with 25 atmospheric layers structure. The spatially gridded annual emissions from GIS are verified to follow most of the spatial distribution pattern of INTEX-B gridded emission in 0.5 by 0.5 degree (~55 by 55 km) resolution. A successful CMAQ test run indicates the results are compatible with air quality models. To sum up, our new emission gridding process could be applied for regions without source specified emission inventory to prepare the model-ready emission input with confidence. In addition, the process to generate the four-domain emission inputs (27/9/3/1km) for Pearl River Delta region has been presented as a study case.

TABLE OF CONTENTS

LIST OF TABLES

Table Page

LIST OF FIGURES

Figure Page

CHAPTER 1
INTRODUCTION

1.1 Asian Emission

Asia, especially East and Southeast Asia, including China, has developed rapidly in the past decade. From the year 2001 to 2006, China's gross domestic product (GDP) increased about 8% ~ 10% annually. This trend is expected to continue in the future. [NBS, 2007] Compared to other continents, the anthropogenic emissions from Asia are dominant due to the fuel consumptions increasing with the dramatic economic growth, as well as relatively low penetration of control technologies. [Akimoto, 2003] Asia brings most of the expected increase (more than 50%) of global NOx emissions during the period from 2000 to 2020. [Zhang, et al., 2007] More than 10% of current global anthropogenic NOx emissions came from China. [Oliver et al., 1996, 1999]

Recent tropospheric satellite observation studies suggested that there are significant increases in atmospheric emissions over Asia. The tropospheric NO_2 abundance over East Asia from 1996 and 2002 has been confirmed by space-based observation from Global Ozone Monitoring Experiment (GOME). [Irie et al., 2005] Richter et al [2005] have retrieved the tropospheric column amounts of nitrogen dioxide from GOME and another satellite instrument Scanning Imaging Absorption Spectrometer for Atmospheric Cartography (SCIAMACHY) over the years 1996 to 2004. They have detected a significant increase of about 50% during this period over the industrialized areas of China. Moreover, the annual growth rates showed an impressively accelerated trend.

However, it is comparatively hard to understand the real emission situation in Asia as their detailed emission rates and statistics are rarely available in public documents. There are relatively less emission inventories in Asia. Most countries, like China and India who are major contributors of Asian emission, have no source-specified emission inventories. Therefore, for a long period of time, estimates based on fuel consumption and general

emission factors were the only way to approach Asian emissions. But these estimates are subjected to larger uncertainties when compared to those in the United States (US) or European countries.

Recently, some researchers cooperated with local environmental agencies in Asian countries were able to access the existing national emission inventories or detailed emission source information such as the emitter locations, emission rates, and control technology efficiency. [Ohara et al., 2007; Zhang et al, 2007; Zhao et al., 2008] In addition, the validated satellite observations are more and more widely applied to predict the distribution and seasonal variation of Asian emissions. Both of these studies highly improved the understanding of Asian emission and its effect on the world. A literature review based on these studies will be introduced in the next section.

1.2 Literature Review

1.2.1 Overview of Asian Emission Estimates

In light of the uncertainty of Asian emission due to a lack of specified emitter information and national statistics, several regional emission inventories have been set up while some global emission inventories like Global Emission Inventory Activity (GEIA) and Emission Database for Global Atmospheric Research (EDGAR) also include Asian regions. Since the first Asian inventory reported SO_2 and NOx emissions for 1975, 1980, and 1985-1987 [Kato and Akimoto, 1992; Akimoto and Narita, 1994], there are four methods generally implemented for Asian emission estimates up to now: 1) Top-Down; 2) Bottom-up; 3) Inverse modeling; and 4) Forward modeling. All methods above have been verified and considered reliable to some extent with different uncertainties.

Top-Down Method

Basically, Top-Down method is to calculate the emission inventory by multiplying the activity data from economic-sectoral Statistics and emission factors from experiments or extrapolated from other countries like United States, with the consideration of the

efficiency of control technologies and its penetration. Streets et al. [2003] provided the first comprehensive Asian emission inventory using the Top-Down method, which integrated anthropogenic, biomass burning, and biogenic emission from Global Emission Inventory Activity (GEIA), for the base year 2000 in support of the Asian Pacific Regional Aerosol Characterization Experiment (ACE-Asia) [IGAC, 2001] and Transport and Chemical Evolution over the Pacific (TRACE-P) field campaigns. [NASA, 2001] The campaigns were carried out in the spring of 2001 with the purpose to investigate the characterization of gaseous and aerosol species in the pollutant outflows from Asia to the western Pacific Ocean and the effect of the outflow.

To estimate the anthropogenic emission in the TRACE-P inventory, the emission sources were firstly classified into five major sectors: Industry, Transportation, Power generation, Domestic fossil and Domestic biofuel. Within each sector, the calculation by multiplying activity rate with emission factor and the removal efficiency of control technologies implemented has been conducted to estimate annual sectoral emission at a national or regional scale for each economic sector. These top-level national/regional emissions were then broken down into grid-cell level emissions according to the geographic or socio-economic information. For Natural emission like biomass burning, it is calculated based on the wildfire data and satellite observation. The TRACE-P emission inventory covers 22 countries/regions in Asia. It contains nine primary species SO_2, NOx, CO, nonmethane volatile organic compounds (NMVOC), black carbon (BC), organic carbon (OC), NH_3, and CH_4 in national, regional and $1° \times 1°$ (~110 km × 110 km) grid resolution. [Streets et al, 2003]

After developed, TRACE-P emission inventory has been the mainly emission applied for Asian air quality modeling. [Fu et al., 2008; Wang et al., 2008] The magnitude and spatial distribution of this emission inventory has been widely examined in TRACE-P field campaigns. The evaluation of TRACE-P NOx emission for China with observations from ground station and aircraft suggested that 47% increase of China's NOx emission is required to reach a good agreement. [Wang et al., 2004] Also, Streets and Zhang, et al.

[2006] have updated the CO emission of China for the year 2001 with a 36% increase after underestimates of TRACE-P CO emission for China has been recognized through a synthesis of TRACE-P measurements, inverse modeling, and Measurements of Pollution in the Troposphere (MOPITT) satellite retrievals. These evaluations indicated that the top-down method most likely led to higher uncertainties in the estimation of regional emissions because of the absence, or inconsistency, of activity statistics, and simply applying general emission factors to major sectors instead of specified sources. But for regions without more information, the top-down method still could estimate emissions at a reasonable magnitude. According to the intercomparison between TRACE-P emission data to the national emission inventory of Japan EAGrid-2000 [Kannari, 2007], the TRACE-P data is consistent with differences smaller than 10% for SO_2, NOx, NMVOC, CO_2, and 30% for CO and NH_3. The $0.5° \times 0.5°$ (~110km × 110km) grid-based emissions from the two inventories match well for NOx, NMVOC, CO, and $PM_{2.5}$, even though the spatial allocation techniques for the local inventory are much more detailed.

In support of NASA's Intercontinental Chemical Transport Experiment Phase B (INTEX-B) experiment, the latest anthropogenic emission inventory, INTEX-B emission inventory, for Asia with the base year 2006 has been developed with a technology-based methodology. Emissions are calculated from the combination of activity rate, technology distributions, emission factors in raw gas, and the penetration of emission control equipments. The best available national and regional emission inventories of Japan, South Korea and Taiwan has also been integrated. [Zhang and Streets et al, 2007] Similar to TRACE-P, The INTEX-B emission inventory has been developed in regional/national scale while a gridded form with the resolution of $0.5° \times 0.5°$ (~110km × 110km) in multiple chemical mechanisms has been provided too.

Bottom- up method

The bottom-up method takes advantage of advanced source classification, detailed emitter information and emission factors from monitoring and experiments to build a much more accurate emission inventory with a high level of confidence. In industrialized

regions of North America and Europe, there is good agreement of bottom-up inventory with satellite observations. [Beirle et al., 2003; Martin et al., 2003, 2006; Jaegle et al., 2005; Richter et al., 2005; Kim et al., 2006] In Asia, only Japan, South Korea, Taiwan and Hong Kong have bottom-up or partly bottom-up national/regional emission inventories. [Kannari, 2007; NIER, 2001; HKEPD, 2002] Recently, Zhao et al [2008] has set up a unit-based emission inventory from coal-fired power plants in China with bottom-up method from 2000 to 2005, and projected the emission till 2020.

Inversing Modeling

Inverse modeling for emission estimates has been increasingly applied with the development of space science and validation technology of satellite observation. It makes use of the ground station observation; aircraft field campaigns, and space-based data. Inverse modeling has been conducted for global and regional emission constrained by satellite data. Martin et al [2003, 2006] used the GOME NO_2 columns for 1996-1997 and SCIAMACHY NO_2 data of 2004-2005 in a global three-dimensional chemical transport model (GEOS-CHEM) to estimate the total NOx emissions in East Asia. The results showed a good agreement with satellite data. The shortcoming is the inverse modeling is only applicable for species with a short lifetime like NOx. Otherwise, it is hard to separate the current and historical emissions.

Forward Modeling

Forward modeling can predict emissions relying on available emission inventories as inputs. After being developed, the TRACE-P emission inventory has been used in a forward mode to predict the CO concentrations, which can then be compared with TRACE-P and satellite observations to derive the apparent CO sources strength. The results of these studies suggested that the order of CO emission in China should range from 140 to 200 Tg/yr. [Heald et al., 2003]

1.2.2 Spatial Allocation

The estimated Asian emission inventory are always in regional or national scale while for air quality modeling, the grid level emission is need. Spatial allocation is a process to break the emissions at the administrative unit level (e.g. county, province or nation) into grid-cell-based emission inputs for air quality modeling. Dai and Rocke [2000] have firstly brought in this concept during mapping the county level area emission to the sub-county level or grid cell level through Geographical Information System (GIS). For this process, the spatial allocation factors have been derived from the spatial intensity based on geocoded source activities. Dai and Rocke also integrated a statistical model using available data like census, employment density, highway information and urban landuse to predict the spatial distribution of source activities. The predicted distribution fits that of the source activities in study area reasonable well. In United States, the Multimedia Integrated Modeling System (MIMS) Spatial Allocator [UNCC, 2003] is free to public to generate spatial surrogates for emissions spatial allocation process in Sparse Matrix Operator Kernel Emissions project (SMOKE) without GIS. The MIMS Spatial Allocator are designed to prepare the area, mobile and biogenic spatial surrogates using the following formula:

$$\mathrm{Srg(Cty,GC)}=\frac{\mathrm{Wt(Cty}\cap\mathrm{GC)}}{\mathrm{Wt(Cty)}}$$

Where,

Numerator: weight attribute in the area of intersection between the grid cell and county;

Denominator: weight attribute in the entire county;

According to its definition, the sum of surrogates for each county should be 1. In US, the weight attributes are based on number of points, length of lines, or area of polygons (e.g. port berths, railroads, population) [UNCC, 2003]

Due to the lack of source activity statistics in Asia, Woo et al [2003] has generated the spatial allocation factors based on population information in 2000 and road network from Digital Chart of World (DCW) to mapping the Asian regional emission into gridded

emission with a resolution of 36km × 36 km with the similar method to MIMS Spatial Allocator.

1.2.3 Carbon Bond Mechanism

In most photochemical air quality models, reduced versions of chemical mechanisms have been implemented with the consideration of computational efficiency to provides a basis for computer modeling studies of ozone, particulate matter (PM), visibility, acid deposition and air toxics issues. These simplified mechanisms are lumped or approximated with a smaller number of reactions through following strategies: mathematical lumping, molecular lumping, or structural lumping. The Carbon Bond-IV (CB-IV) Mechanism, a hybrid mechanism of explicit chemistry, surrogate approximations, and lumped or generalized chemistry, was developed in late 1980s mainly for urban and regional photochemical atmospheric modeling. [Gery et al., 1989; Isukapalli, 1999] Updates have been made to CB-IV like PAN chemistry, radical termination reactions, and isoprene chemistry etc.

An updated version of Carbon Bond-IV in 2005 (CB05) has been implemented to the new released Community Multiscale of Air Quality Modeling System (CMAQ) version 4.6. Comparing to CB-IV in previous CMAQ models, an extended inorganic reaction set and explicit organic chemistry for methane and ethane has been added in CB05. The number of chemical reactions and species in CB05 are 156 and 51 respectively while in CB-IV are only 93 and 13. The new introduced VOC species and reactions improve the simulation performance of atmospheric oxidant chemistry based on a CMAQ modeling of Continental United States (CONUS) and evaluation of chamber data from University of North Carolina (UNC) and University of California, Riverside (UCR). In the CMAQ modeling case, the incorporation of CB05 increases in ozone prediction by about 14% when compared to CB-IV, but didn't change the time of peak ozone occurrence. It decreases in the prediction of aerosol sulfate, aerosol nitrate and organic aerosol by about 8%, 3% and 10%, respectively. In addition, the model run time increases by about 28%.

[Yarwood et al., 2005] These changes brought in by CB05 made it necessary to prepare the emission input for CMAQ in this updated mechanism.

1.3 Problems

There are three problems that give cause for concern. First of all, the most recent studies for Asian emissions focus solely on anthropogenic emissions. Ohara et al [2007] developed a dynamic emission inventory for Asia from 1995 to 2004, which shows the trends of only anthropogenic emission. INTEX-B emission inventory, which is thought to be the latest and the most accurate reflection of recent Asian emission only accounts for anthropogenic emission. [Street and Zhang et al., 2007] There is no emission inventory after TRACE-P considering both anthropogenic and natural emissions. Secondly, a new chemical mechanism Carbon Bond IV 2005 has been implemented in CMAQ 4.6 and will be the only VOC mechanism in upcoming CMAQ 4.7. However, most Asian emission inventories available are still using CB-IV species. Currently, there is no model-ready emission input with fine enough resolutions in CB05 mechanism for Asia. More importantly, the resolutions of current emission data are not fine enough for regional air quality modeling. For example, INTEX-B emission data has a resolution $0.5° \times 0.5°$ (~ $55\ km \times 55km$), which is quite coarse for regional or urban modeling, of which the horizontal domain resolutions are usually 4km or 12km.

1.4 Purpose

In light of this situation, our purpose is to develop the latest gridded Asian emission input with multi-finer resolution based on best available Asian emission inventories, INTEX-B 2006 regional emission inventory, biogenic emission from GEIA, ship and biomass burning emission from TRACE-P, for regional air quality simulation and prediction in eastern Asia. A GIS-FORTRAN based system has been established to prepare the model-ready emission inputs in multiple resolution and domain configurations with more flexibility for air quality modeling from regional or global annual emission. In this study,

the process and analysis of emission inputs data prepared for the Pearl River Delta Region will be presented as an example. Also, a new set of spatial surrogates files will be constructed for Asia. On the other hand, a comparison to INTEX-B gridded emission in $0.5° \times 0.5°$ resolution has also been conducted to investigate the accuracy of spatial allocation.

1.5 Thesis Structure

Chapter 1 introduced the background and previous researches carried out on Asian emissions, as well as the study objectives. Chapter 2 will focus on the "Top-Down" methodology for spatial allocation applied in this study based on best available emission inventories, geographic features and socio-economic information. The step-by-step procedures, including GIS processing and FORTRAN programming, will also be illustrated, as well as the input data sources. The generation and implementation of spatial allocation factors will be introduces with examples in PRD region. The gridded emission and spatial allocation factors results will be analyzed and discussed in Chapter 3. Chapter 4 is the conclusion and recommendations for further work.

CHAPTER 2
METHODOLOGY

2.1 Flowchart

Fig. 1 (All figures are in Appendix) shows the flow chart of the emission gridding process, which can be divided into two major modules based on the two computer technologies applied: Geographic Information System (GIS) and Computation with FORTRAN code. The left side shows the general steps to spatially and temporally grid the annual regional emission inventory down to hourly gridded emission in network Common Data Form (NETCDF) format, which could be directly used as model inputs for most photochemical air quality modeling like CMAQ or Comprehensive Air quality Model with eXtensions (CAMx).

The right side is the detailed procedures. As mentioned in Section 1.4.1, we use both anthropogenic and natural emission as inputs for our gridding process study. Firstly, the annual anthropogenic emissions at regional scale of each sector have been broken down into the finest grid cell size according to the spatial allocation factors. They are pre-generated from the socio-economic information and geographic features such as population, road network, and land cover. At the same time, the annual global natural emission (in much larger grid resolution) has been extracted and interpolated into the same finest grid cell size. For biomass burning emission with TRACE-P chemical species, a speciation mapping process is also required to ensure the chemical species of all gridded emissions are consistent with that in air quality models. Then, the gridded emissions are aggregated up to the desired grid cell sizes for each domain, respectively. After that, all grid emission datasets are changed to the projected coordinates system, which needs to be consistent with specific air quality models, and extracted for the predefined domains. After exporting data from the GIS program, the annual gridded emission data of each sector are combined and projected to the different vertical layers according to the stack heights and projection energy in a FORTRAN-based module. In

this module, the combined annual emission will be allocated to hourly emission with the temporal profile. In the end, the hourly gridded emission will be formatted exported as model-ready emission inputs for air quality model.

In the sections that follow, the configurations, data sources and the details of each procedure will be elaborated. The spatial allocation process and the preparation of spatial allocation factors will be introduced in detail. The intermediate outputs for each step will also be presented.

2.2 Configurations

2.2.1 Domain

A mother domain has been defined for East, Southeast, and Central Asia, as well as four nested domains for the CMAQ modeling system. The domain has been configured from three aspects: coordinates system with projection parameters, horizontal domain extents, and vertical structure.

Coordinates System

All emission development for the mother domain is in the non-projected coordinates system, which means the map unit is *degree*. This increases the flexibility and accuracy for transformation among different projections. With this consideration, it is easier to provide gridded emissions of other Asian regions without rebuilding the whole gridding system, which is time consuming.

Lambert Conic Conformal (LCC) projection appropriate for simulating the meteorology and air quality for Pearl River Delta (PRD) region has been adopted for the modeling domains. To minimize the distortion from projection transformation from a non-projected coordinates system, parameters were therefore defined such that the region of interest lies between the two true latitudes of the projection system. The parameters in Table 1 (All tables are in Appendix) have been applied according to the geographic extent of

modeling domains. For future reference, this projection parameter, especially the two standard parallels, or true latitudes (*alpha* and *beta* in Table 1) may vary with different regions studied.

Horizontal domain settings

The target mother domain is defined with the consideration of the coverage of INTEX-B 2006 emission as well as our modeling domains. We hope the mother domain could cover all countries/ regions included in the INTEX-B emission inventory. Then we can zoom into any particular regions interested in the future with nested domains. Therefore, the geographic extent of the mother domain is determined as 13º *S* ~54 º *N* in latitude and 60 º *E* ~158 º*E* in longitude, which contains totally 22 countries/regions) in East, Southeast and Central Asia. (See Fig. 2 (a)) Our four modeling domains in resolutions of 27/9/3/1km (~13.5/4.5/1.5/0.5 arc minute) have been defined with the coordinates of their four corners in Table 2. Fig. 2 (b) displays the geographic extents of four nested modeling domains.

Vertical Structure

In this study, we adopted the vertical structures of 25 vertical atmospheric layers defined according to the meteorological modeling in Mesoscale Modeling System Generation 5 (MM5) and Weather Reasearch Forcasting Model (WRF). (See Table 3) But for our GIS-FORTRAN based system, it could be use-defined when needed.

2.2.2 Speciation

As the latest Carbon Bond IV 2005 (CB05) chemical mechanism has been implemented into CMAQ 4.6 model, the CB05 with $PM_{2.5}$ speciation has been applied for this study. In emission input, there are 16 CB05 species while the CB-IV has ten VOC species (See Table 4). [Yarwood et al., 2005]

2.2.3 Base year & Episodes

The base year for this gridding process study is 2006 according to the INTEX-B emission inventory. Four episodes in different seasons have been selected for CMAQ modeling. The longest episode is from September 1st to October 12th including nine initialization days. The other three episodes are in January, March, and November, respectively.

2.2.4 Hardware and software requirements

The ArcView 3.3 with Spatial Analysis 2.0 for Windows XP operation system (OS) is the primary processor for spatial allocation and the allocation factors' generation. Due to the vast domain coverage and extremely fine resolution, the normal performance of spatial allocation requires RAM size to be at least one gigabyte for a single Personal Computer. Otherwise, the process will be very slow and fragile. The FORTRAN 90 with pgf90 compiler in Linux OS has been used for matrices computation.

2.3 Data sources

2.3.1 Anthropogenic Emission

Basically, the INTEX-B 2006 regional emission inventory [Streets and Zhang et al., 2007] and TRACE-P ship emission [Streets et al., 2003] have been used as the anthropogenic emission inputs for this study. The INTEX-B emission dataset contains regional/national emission inventory in ten primary species: SO_2, NOx, CO, BC, OC, $PM_{2.5}$, PM_{10}, NMVOC, CH_4, and NH_3, while NMVOC includes 16 CB05 NMVOC species. Except for NH_3 and CH_4 emission, all species are classified into four major sectors: Industrial, Residential, Power Generation and Transportation. (See Fig. 3)

The NH_3 emissions are categorized in more detail to six sub-sectors: Cattle, Pigs, Other Animals, Fertilizer Use, Bio-fuel Use, and Other Sources. The CH_4 emissions are categorized into seven sub-sectors: Rice Cultivation, Animal Emissions, Landfill, Wastewater Treatment, Coal Mining/Combustion, Oil/Gas Extraction and Use, and Bio-

fuel Combustion. As the two species are not categorized in the same four sectors as other species, to simplify the spatial allocation processes in ArcView, the NH_3 and CH_4 emissions are treated as two species in a new sector of livestock seperately. Then for the other species, we can spatial allocated with batch process by sector. The livestock sector is at the same level of the industrial or transportation sector, though the emissions of the two species also come from other sources. The ship emission is also accounted for in the anthropogenic emission as it is from human activities. We combined the TRACE-P ship emission as a separate sector 'ship' in this study. (See Fig. 1)

2.3.2 Natural Emission

In order to reveal the actual atmospheric emission, the biomass burning, and biogenic emissions have been integrated into the emission data ptocess. We adopted the 2000 TRACE-P biomass burning and biogenic emission from GEIA into our new emission inventory. Both are gridded global emission inventory with the resolution of $1° \times 1°$ (~110km × 110km). For biogenic emission, there are three species: isoprene, terpene, and Other Volatile Organic Compounds (OVOCs) while the biomass burning emission is in TRACE-P species.

2.3.3 Administrative Boundary

The administrative boundary is in ESRI shapefile format while each polygon shape in the file is an administrative unit, usually a country or region like province. Most administrative boundaries for each country/region have been extracted from the Regional Air Pollution INformation and Simulation - Asia (RAINS-Asia) model, the Digital Chart of the World (DCW) [Defense Mapping Agency, 1989] and TRACE-P emission program. [Streets et al, 2003] Comparing to TRACE-P emission program, we distinguished Chengdu Municipality from Sichuan Province in China based on INTEX-B administrative boundaries.

2.3.4 Population: LandScan

The LandScan 2006 population dataset with a geographic coordinates system from Oak Ridge National Laboratory (ORNL) has been adopted to provide population distribution information. ORNL began developing the LandScan population database in 1998. They integrated all effect factors and indicators like transportation networks, slope, land cover, populated places, nighttime lights, exclusion areas, urban density, coastlines, and the best available census counts, taken from a GIS and Remote Sensing (RS) technologies or social survey, to model the global population distribution. LandScan 2006 population dataset is an ESRI raster grid in 30×30 arc-second (~1km $\times$ 1km) resolution with global coverage. [LandScan, 2006] Fig. 4 shows the population distribution for Southeast Asia extracted from LandScan 2006 and a detailed display in the PRD region.

2.3.5 Road Network

Road Network is the key factor to determine the distribution of emission from the transportation sector. Unlike US, there is no Vehicle Miles Traveled (VMT) or Average Daily Traffic (ADT) information in Asia. Only the road length has been considered as an indictor of spatial distribution of mobile emission. The 2003 Chinese classified road network from the Chinese consulting agencies is used for Chinese regions. It includes five types of roads: high speed, national, provincial, urban, and town. For other Asian countries, road networks in the Digital Chart of the World (DCW) are adopted. [ESRI, 1997] Both datasets are polyline shape files and have been merged into one shape file in this study (as Fig. 5 displays) to generate the spatial allocation factors for emission in the transportation sector. We use the ship lane from TRACE-P since updated Asian ship lane information is under development.

2.3.6 Land Cover and Land Use

The Land Cover and Land Use (LCLU) information has been extracted from Global Land Cover Characteristic Database version 2.0 (GLCC v2.0) available at United States Geological Survey (USGS) Earth Resources Observation and Science Center (EROS) for our mother domain. [Loveland, 2000] It is derived from the 1-km Advanced Very High Resolution Radiometer (AVHRR) data spanning a 12-month period (April 1992-March 1993). Like the LandScan dataset, it is also a raster grid in 30 by 30 arc-second (~1km × 1km) resolution without projection. [USGS, 2005] For coverage we concerned, there are 22 land cover types as Table 5 shows. Fig. 6 shows both an overview and a detail display of the land cover in Asia.

2.3.7 Large Point Sources

The emission sources in large power plants always have high emission rates and elevated emission height, like stacks of power plants and industrial facilities. They will be treated as large point sources (LPS) during the gridding process. However, it's different from the point sources in US as there is no monitoring information like emission rates, velocity and removal efficiency of control equipments, which means there is no plume calculation and the LPS emission in Asia is not hourly data. For China, currently the plants with 1000MW installation capacities or more are considered as LPS in our study since the information of smaller plants is hard to obtain. Their installed power capacities and annual power generation in 2005 were collected from the 'Chinese Electricity Statistical Yearbook 2006' and 'Statistical Materials for Chinese Electrical Industry'. [2006] The coordinates of LPS locations have been obtained from Google Earth. The information of LPS in other Asian regions was extracted from the RAINS-Asia. Fig. 7 shows the distribution of total 163 LPS in Asia.

2.4 Pre-process

The pre-process includes all preparation before starting gridding process to ensure the consistency of emission species in each sector and improve the efficiency and flexibility. There are three major tasks: 1) Develop a mapping table to convert the biomass burning emissions species in TRACE-P speciation to CB05 VOC with $PM_{2.5}$ speciation. 2) Split emission of LPS from Power generation sector. 3) For natural emission already spatially gridded, interpolated to our finest grid resolution.

2.4.1 Chemical mapping cross-reference table

A mapping table converting TRACE-P species to species in CB05 VOC with $PM_{2.5}$ speciation has been established for the biomass burning and ship emissions. (See Table 6 and Table 7) These tables also provide the mapping factors from particular matter ($PM_{2.5}$, PM_{10}, BC and OC) in different sectors to species in CMAQ $PM_{2.5}$ speciation. [Middleton and Stockwell, 1990; Stockwell et al., 1997; Jacobson, 2000, 2002; Sexton and Jeffries, 2002; Yarwood et al., 2005]

2.4.2 Split POW emission

We split the power sector of INTEX-B emission inventory into two sectors: LPS and small power plants (POWS). LPS are typical point sources while the other small power plants are treated as area sources in this study as they don't have high stacks. Plus, there are thousands of the POWS. Currently, to identify their locations and emission rates are unpractical.

For each administrative unit, the POWS emissions equal to the power sector emission in INTEX-B subtract the total emission from LPS in this unit. With the assumption that the emission has a linear correlation with annual power generation, we estimated the emission of a LPS through multiplying the total power emission within one administrative unit where the LPS located with its power generation ratio. The power

generation ratio is defined as power generation of a LPS divided by the total power generation in the administrative unit where the LPS is located. For China, the latest regional power generation for year 2005 has been acquired from the 'Thermal Power Generation By Region' table in "Chinese Electricity Statistical Yearbook 2006" [2006]. For other Asian regions, we adopted the power generation ratio in TRACE-P.

2.4.3 Natural emission interpolation

The natural emissions have been generated based on land cover, meteorology and wild fire information. They are spatially allocated already in $1° \times 1°$ (~$110km \times 110km$) resolution and point shape file format. This means the emission value of a grid has been geographically stored at the point in the center of the grid. In this study, we applied the interpolation function in ArcView to convert the natural emission to raster grids in our finest resolution $0.5min \times 0.5min$.

After pre-process, we have summarized a new emission inventory classified in nine sectors: industry, residential, transportation, LPS, POWS, ship, livestock, biogenic and biomass burning.

2.5 Spatial Allocation

To spatially allocate the regional emission into each grid, the concept of spatial allocation factors have been introduced. In this study, we achieved the purpose of spatial allocation through the following formula showing the general idea of how to allocate the regional/national emission to gridded emission:

$$EI_{grid} = EI_{unit} \times AF_s$$

Where, EI_{grid}: the annual emission for each grid;
EI_{unit}: the annual emission for the administrative unit in which the grid is included;

AF_s: the spatial allocation factor representing the emission portion one grid occupied in the administrative unit within which it located.

Spatial allocation factors, like spatial surrogates in SMOKE, is a ratio of the emission from one gird on an administrative unit basis, usually a region or country in this study. Spatial allocation factors are generated mainly based on the geographic features such as land cover and road network, as well as socio-economical statistics like population and power generation of large point sources. The basic definition of spatial allocation factor is:

$$AF_{i,n} = \frac{W_{i,n}}{W_{i,m}}$$

Where,

$AF_{i,n}$: Allocation factor for n^{th} grid based on feature I;

$W_{i,n}$: Weight of feature i in n^{th} grid;

$W_{i,m}$: Weight of feature i in m^{th} polygon (always an administrative region) which contains nth grid.

From its definition, it is known that all types of the surrogates are dimensionless and range from 0 to 1.

The geographic features and socio-economic information can be categorized into three formats: point, polyline and raster grid, which are use to allocate the point, mobile and area emission sources respectively. The surrogates for point sources are generated from point features like LPS. The mobile spatial surrogates are applied for the transportation emission and generated from the road network. The area spatial surrogates are generated for the residential, industry, POWS and livestock emissions. They are generated from population or land cover and land use datasets. In this study, all allocation factors except spatial allocation factors based on LPS information will be created in raster grid format to improve the performance of spatial computation in ArcView due to our large domain size and fine resolution.

2.5.1 Population AF

The allocation factor based on population (AF_pop) is generally defined as:

$$AF\_pop_n = \frac{Count_n}{Count_m}$$

Where,

AF_pop_n: Allocation factor for n^{th} grid based on population;

$Count_n$: people count in n^{th} grid

$Count_m$: Total people count in m^{th} polygon (an administrative unit), which contains n^{th} grid.

2.5.2 Urban/Rural AF

There is much information available to detect urban areas such as population density, land use and nightlights relying on the remote sensing technology. Since our ultimate objective is to generate the allocation factors of urban and rural area in 30 by 30 arc-second (~1km × 1km) resolution, the most effective and feasible way is to define urban/rural area based on population density with the LandScan 2006 dataset. The definition of urban area based on population density always varies among different countries. In this case, a LandScan grid cell with population density larger or equal to 1500 person per square kilometers has been defined as urban grid. [Liu et al, 2003] After urban area has been detected, an urban/rural mask in raster grid format has been used to filter out the urban population and rural population from LandScan. Fig. 8 shows both urban and rural population in PRD region as an instance. The complementary area between the two is evident. With these two datasets, urban/rural allocation factors could be created with the definition as follow:

$$AF\_rural_n = \frac{Count_{n,r}}{Count_{m,r}}$$

$$AF\_urban_n = \frac{Count_{n,u}}{Count_{m,u}}$$

Where, AF_urban_n: the allocation factors for n^{th} grid based on urban population;
AF_rural_n: the allocation factors for n^{th} grid based on rural population;

2.5.3 Cropland AF

The LCLU data is mainly applied to generate the spatial surrogates for NH_3 and CH_4 emissions. Considering about the farming and agriculture situation in Asia, the NH_3 and CH_4 emissions from sectors like biofuel use, landfill, and wastewater treatment etc are thought less LCLU related but more human activities related. For example, most grassland in Tibet of China is not used for raising cattle, as the population density there is very low. Therefore, the spatial allocation of these sectors will be reasonable to generated from the population or urban/rural population. An allocation factors reference table (see Table 9) has been provide to demonstrate the detailed assignment information.

The cropland allocation factor based on LCLU is defined as:

$$AF\_crop_n = \frac{A_{n,c}}{A_{m,c}}$$

Where,
AF_crop_n: Allocation factor for n^{th} grid based on crop landcover corresponding to LULC ID 2, 5 and 6;
$A_{n,c}$: Area of Crop landcover in n^{th} grid
$A_{m,c}$: Total area of Crop landcover in m^{th} polygon (always an administrative region), which contains nth grid.
In this study, the coverage in LCLU with category ID 2, 5 and 6, which are Dryland Cropland and Pasture, Cropland/Grassland Mosaic and Cropland/Woodland Mosaic respectively, has been extracted for AF_crop. The LCLU coverage with ID 3, which is

recognized as Irrigated Cropland and Pasture, has not been extracted, as they are mostly the parks while comparing to the land cover map in big cities like Beijing and Hong Kong.

2.5.4 Road network / ship AF

The allocation factor based on road network or ship lane is defined as:

$$AF\_rd_n = \frac{Length_{n,\,rd}}{Length_{m,\,rd}}$$

$$AF\_ship_n = \frac{Length_{n,\,sp}}{Length_{m,\,sp}}$$

Where,

AF_rd_n: Allocation factor for n^{th} grid based on road network;

$Length_n$: Road / ship lane length in n^{th} grid

$Length_m$: Total road /ship lane length in m^{th} polygon (administrative unit), which contains nth grid.

The subscript 'rd' represents road while 'ship' represents ship lane.

Though the AF_ship is defined above, in this case we adopted the AF_ship from TRACE-P program, as the shiplane information is not available. The AF_ship from TRACE-P has a resolution of 2×2 min (~$4km \times 4km$)

2.5.5 LPS AF

The LPS surrogates is actually the annual power generation ratio associate with each LPS defined below:

$$AF\_LPS_N = \frac{APG_N}{APG_T}$$

Where:

N: the ID of LPS;

AF_LPS_N: the surrogate for Nth LPS;

APG_N: the annual power generation of Nth LPS;

APG_T: the total annual power generation of the whole region which the Nth LPS located in.

Table 8 and Table 9 summarize: 1) which allocation factors will be applied to spatially grid emissions for specific sector or species; 2) based on which dataset the allocation factors are generated. Generally, we use AF_LPS for spatial allocation of LPS emission while AF_pop has been applied for POWS since the power generation mainly depends on the population in Asia. Certainly, the AF_pop has been used to allocate the residential emission, as it's more human daily life related. The AF_rd and AF_ship have been implemented for emission from transportation and ship sector respectively. In Asia, most regions are developing countries where the industry is concentrated in or around the urban area so that AF_urban has been applied. The situation is more complicated for NH_3 and CH_4 emission as they are classified in more sectors. For the emissions from Landfill, Wastewater Treatment, Oil and Gas Extraction and Use, in which sector the activities only occurred in urban area for developing countries in Asia, AF_urban has been used for their spatial allocation. For emissions from Farming or Agriculture activities like Animal emissions, Cattle, Pig, Other emission and Biofuel Use, AF_rural has been applied. For emission from Rice Cultivation and Fertilizer Use, which mainly depends on the area of cropland, AF_crop has been adopted. For emission from other sources that are not clear, we assume they are population related and AF_pop has been used.

2.6 Projection Transformation

After spatial allocation, the gidded emission data have been changed to the predefined LCC projection and extracted to the nested domains for export. Projection transformation always causes the distortion that may 'shift' the grid from the original place. To reduce this effect, two measures have been implemented. Firstly, we changed the unit of gridded

emission from ton per year per grid (ton/yr/grid) to kilogram per year per square kilometers (kg/yr/sq-km). Then the projection transformation has been implemented to the emission density grids instead of emission grids whose value located in the center of each grid. Secondly, a resampling process supported by ArcView Spatial Analyst has been conducted after the projection transformation to uniform the gird size from degree by degree to kilometers by kilometers. This process has been widely used in GIS application to interpolate cell values when transforming raster grids to a new coordinates space and cell size. [ESRI] The emission value of a grid will be recovered by multiplying the emission density with grid area later.

2.7 Combination and Vertical Distribution

The sectoral emission data exported from the GIS system will be combined. This combine is not a simple sum up. Emissions from different sectors have different emitting height or energy. They will be projected to the different vertical layers through a FORTRAN program based on the stack height or general emitting energy. The stack heights of power plants in China are ranging from 150 to 220m determined by local regulations while 36m in South Korea. [Woo et al., 2003] Table 10 shows the vertical distribution ratio of each sector, which is simply interpolated with the layer heights based on the 14 vertical layers set in CMAQ modeling for Beijing Olympic Games [Streets and Fu et al., 2007]

2.8 Temporal Allocation

The temporal allocation of spatially gridded emissions is to convert the annual emission to hourly emission inputs for air quality modeling purpose. For anthropogenic emissions, the hourly allocation ratio profile adapted from TRACE-P program is based on the study of emission seasonality, weekly and daily human activity variation. It is generated from the average fractional hours of stove operation in capital cities of 31 provinces in China, which depends on the fuel combustion activities and outdoors temperature. [Streets et al.,

2003; Wang et al, 2005] The monthly variation, daily variation in a week and hourly variation in a day has been considered. But among weeks in the same month, the temporal profile is flat due to the lack of local measurement data. For biogenic emissions, the monthly temporal profile has been obtained from GEIA and the daily and hourly temporal profiles are the same as the TRACE-P due to lack of measurement data. For biomass burning, the monthly temporal profile has been adopted from TRACE-P based on the satellite observation and wildfire data. Similar to spatial allocation factors, the temporal allocation factors multiply the gridded annual emission from spatial allocation to generate the hourly emission inputs for CMAQ.

$$EI_{hr} = EI_a \times R_{temp}$$

Where EI_{hr} is the hourly emission inventory for each grid cell;
EI_a is the annual emission inventory for each grid cell;
R_{temp} is the temporal allocation ratio for each grid cell.
For consistency consideration, the Greenwich Mean Time (GMT) has been used.

2.9 Export and Visualize

After temporal allocation, the hourly, spatially gridded emission data for total 29 species in CB05 w/ $PM_{2.5}$ speciation have been written to standard NETCDF file through Input/Output Applications Programming Interface (I/O API). These model-ready outputs can be visualized and analyzed by several softwares while in this study, we chose Package for Analysis and Visualization of Environmental data (PAVE). Due to the finer resolution and more vertical layers that markedly increase the file size, it is not recommended to store hourly emission data more than one day in a single NETCDF file. Otherwise, the program will stop when file size reaches four gigabyte.

CHAPTER 3
RESULTS AND DISCUSSION

3.1 Spatial Allocation Factors

In this study, we have developed the spatial allocation factors based on population, road network, land cover and land use. Fig. 9 through Fig.15, display the spatial allocation factors for the whole mother domain and some megacities in which many people have demonstrated an interest. In Fig. 9 and Fig.13, high values of AF_pop and AF_rd appear as expected in megacities like Beijing, Tianjin, Shanghai, Hong Kong, Tokyo and the western coastline of Taiwan. Fig. 9 and Fig.10 show the AF_urban and AF_rural, respectively, which indicates a successful partition of urban and rural areas.

With regard to the AF_crop, a surprisingly high value is shown in the forenamed megacities where there is little land set aside for agricultural use (See Fig. 12). This anomaly is due to the definition of AF_crop, which is the area of an agriculture land grid divided by the total area of agriculture land in this region. Unlike population or road network, the area value of each grid cell in LCLU dataset is almost the same. The resulting high AF_crop values just illustrate there is little agriculture land in these megacities. That being the denominator, the agricultural land areas in these megacities are small. Taking this information into account, Fig.12 accurately shows a reasonable agriculture land distribution. Using China as an example, the AF_crop represents a large coverage in southeast China (including Sichuan, Chongqing, Hunan, Zhejiang, and Guangxi) that is the main rice production area of the country. A similar situation occurs in north China where Shanxi, Hebei, Liaoning and Jinin provinces are the main wheat production areas of the country.

The AF_LPS are calculated and associated with the exact point source. (See Fig. 14) In China, where LPS data has been updated to the year 2005, most LPS are located in the

northeastern or eastern areas. Fig.15 displays the distribution of AF_ship, which looks similar to its relevant geo-features. The AF_ship goes through the Sea of Japan, thence on to the East China, South China, and Philippine Sea on the east side, thereafter, along the western coastline of India on the other side.

3.2 Emission Aggregation

Fig.16 showing the dynamic change of gridded NOx emission values in residential sector while aggregating the finest grid cells to coarser resolutions in PRD region. The finer grid resolution (Fig.16 (a)) is capable to reflect the emission spatial distribution for small regions while the coarser resolution (Fig.16 (d)) tends to lose the spatial distribution pattern for small administrative units.

3.3 Annual Emissions Distribution

Fig. 17 shows the comparison of spatial distributions of our gridded anthropogenic and sectoral annual emission to INTEX-B gridded emission in resolution of $0.5° \times 0.5°$ (~55km × 55km). To verify whether our GIS-based spatial allocation method can distribute the emission to grid cell appropriately, we aggregated our annual anthropogenic emission (without biomass, biogenic, and ship emission) to $0.5° \times 0.5°$ (~55km × 55km), which is the same resolution as the INTEX-B gridded emission. Now the spatial distribution and magnitude between the results based on our top-down method and INTEX-B gridded emission are comparable. Species compared includes NOx, SO_2, $PM_{2.5}$ and PM_{10}.

The results shown in Fig. 17, suggested that our GIS-based method performed fairly well in capturing the spatial distribution pattern of INTEX-B gridded emission. The distribution of our gridded NOx annual emission is the same as that of INTEX-B in India, Japan, most of China, and other Southeastern countries. Only in South Korea, our results were slightly less than expected. However, for all NOx, $PM_{2.5}$, and PM_{10} in INTEX-B

emission, there is obvious high emission concentrated at Ulaanbaatar, capital of Mongolia, which our results were unable to replicate. To investigate this difference, we confirmed the INTEX-B gridded emission on a sectoral basis for these three species. (See Fig. 18 ~ Fig. 20) It is found that the concentrated high emission for NOx is attributable to the power emission while the residential emission is responsible for that in $PM_{2.5}$ and PM_{10} emission. (See Fig. 18 to Fig. 20) Referring to our allocation factors based on population and LPS, there is no LPS or high population density at Ulaanbaatar that emission will not be allocated into this area. This is the main reason for the difference between our results and the INTEX-B. Since there is no detailed documentation about how INTEX-B developed gridded emission, a more detailed local emission inventory, if available, is needed to validate our methodology and the spatial allocation method INTEX-B applied.

In summary, the comparison of our results to the INTEX-B gridded emission of four species shows that our results follow almost the same spatial distribution pattern for all parts of Asia excluding Mongolia. It is then diagnosed that this misallocation comes from the spatial allocation of emission in the power and residential sectors. For the power sector, no detailed information regarding the number, exact location, annual emission rate, and abatement technologies implemented of LPSs is thought to be the most likely reason for the large difference in some regions. For example, we only selected LPS with an installed capacity larger than, or equal to, 1000MW in China. For the residential sector, we use the AF_pop that succeeds in spatial allocation for most regions. A more detailed local emission inventory is needed to determine whether the method to spatially allocate the residential emission with population information is applicable here or not.

3.4 Model Ready Emission and Test Run

Fig. 21 to Fig. 24 shows the model-ready SO_2 emission outputs for four domains in different layers of interest. It also presents the daily temporal variation by comparing the emission in the first layer at 4:00 GMT (a) to that at 16:00 GMT (b), which are 12:00 pm

(noon) and 24:00 am (midnight) of Beijing time, respectively. The obvious emission difference due to human activity level could be observed. The visualized gridded emission could provide information for decision makers to control regional emission as well. Taking the domain 1 (D1) as an instance, Fig. 21 (a) displays the distribution of emission mainly from residential, transportation, and small power plants. The concentrated value in Southwest China (Sichuan and Guizhou provinces) is due to the residential consumption of coal with high sulfur content. [Zhao et al., 2008] Fig. 21 (c) reveals that the emission in the second layer, which is primarily from the industrial sector, is dominant among all layers. Its relatively higher emissions appear on the northeastern and southeastern coastline of China, corroborating the fact that these areas are indeed, more industrialized. Fig. 25 and Fig. 26 shows the CO and FROM emission inputs of four domains for CMAQ modeling.

A one-day CMAQ test run with profile initial and boundary conditions has been carried out for domain 4 (D4, 1km × 1km) with the only purpose to prove that our final outputs, spatially and temporally gridded emission datasets in NETCDF format, could work successfully in CMAQ with the meteorological inputs from MCIP with the same vertical structure. Fig. 27 shows the preliminary CMAQ results for O_3, CO and NOx.

3.5 Comparison with INTEX-B

To conserve the quality of spatial gridding process, a comparison between our results from GIS-based spatial allocation and INTEX-B emission has been conducted. We computed the total emission for each region from our gridded annual emission data in resolutions of1km × 1km through the zonal summary function in ArcView. The zones we used are the polygons of our administrative boundary shape file. This computed regional emission is called as ZonalSum in this study. We defined the following terms to compare the ZonalSum with INTEX-B:

$$\text{Diff} = (\text{ZonalSum}) - (\text{INTEX-B})$$

$$Diff_p = (Diff) / (INTEX\text{-}B)$$

Where,

Diff: difference between our results and INTEX-B;

ZonalSum: sectoral total annual emission of an administrative unit summed up from our gridded emission input from GIS process in resolution of 1km × 1km;

INTEX-B: INTEX-B regional emission inventory

$Diff_p$: Difference between our results and INTEX-B normalized to the INTEX-B regional emission inventory.

Here the NOx emission has been presented as an example. Fig. 28 shows the difference and difference percentage between ZonalSum and INTEX-B. In Fig. 28 (a), the largest difference occurred in China, which has the largest NOx. As Fig. 28 (b) shows, the difference percentages between ZonalSum and INTEX-B are limited to ± 1.5% for all regions, which indicates our spatial allocation process accurately converted regional emission into grid level emission with rare data missing.

Through the same method, we compare the total Asia emission summed from our gridded emission in different resolutions with INTEX-B regional emission inventory. From Fig. 29, it is found: (1) The ZonalSum always less than INTEX-B. This is due to the GIS limitation that the grides crossing the administrative boundary or coastline will be miss placed or not accounted in when the center of the grid lies in the water body. (2) The difference of ZonalSum to INTEX-B increases while the grid resolution increase from 1km × 1km to 27km × 27km. This is caused by the aggregation process, which tends to even the spatial distribution of emission data. (See Fig. 16) (3) The difference percentage ranges from 1% to –7%. The difference in residential sector is the smallest while the largest in power sector. This indicates the AF_pop performs better in spatial allocation of residential emission while AF_LPS may need to improve.

CHAPTER 4
CONCLUSIONS AND RECOMMENDATIONS

4.1 Conclusions

To sum up, we have consolidate the best available regional Asia emission inventory INTEX-B, TRACE-P and GEIA and successfully converted the regional/national emission inventory to model-ready hourly-gridded emission data, with much finer resolutions, through our GIS-FORTRAN-based program. The outputs have worked successfully in the CMAQ test run. They provide a more accurate illustration of the spatial distribution of emissions that could ultimately assist decision makers in their attempts to control regional emissions.

Also, a set of spatial allocation factors with very fine grid cell size has been developed for area and mobile emissions using the most recent geographic and socio-economic information we can access. This allocation factor dataset could be applied in SMOKE as well, while linking to detailed local emission inventory at the county or district level via appropriate identification information, such as, by country-state-county code. Both the spatial and comparison between ZonalSum and INTEX-B indicates that the AF_pop performs fairly well in allocating residential emissions. The AF_LPS is thought to be the reason causing a large difference in the power sector. More detailed information about LPS is required to improve the accuracy of future spatial allocation studies. The comparison analysis also suggested that the aggregation process would cause difference between ZonalSum and INTEX-B during the spatial allocation.

The flexibility, capability, and accuracy of our GIS-FORTRAN-based program in preparing model-ready emission inputs have been proven in this study. GIS has also been proven to be an efficient tool for visualization and statistical analysis for the emission process.

4.2 Recommendation

There are five major recommendations for future work:

(1) The allocation factors based on population (AF_pop) are reliable and can be applied in future studies of spatial allocation of emissions from residential sectors. Further research on extending the application of population data in the emission spatial allocation process is needed.

(2) Only considering power plants with installed capacity larger than or equal to 1000MW is not enough. More detailed information of LPS is required to eliminate the uncertainty in spatial allocation of the power sector. Since the Chinese will gradually phase out small power plants (installed capacity < 300MW), the collection and integration of information about LPS with installed capacity ≥ 300MW is needed.

(3) Considering that the aggregation process will bring larger difference which will be significant to regions with small coverage or emissions, the finer resolution is needed for emission inputs preparation. Plus, it's believed that the difference will be reduced if we develop the spatial allocation factors with difference resolutions (e.g. 27km/9km/3km) and apply spatial allocation for each domain and resolution instead of simple aggregation.

(4) Sensitivity studies among different allocation factors are a potential way to understand the emission characteristics in each sector. Various schemes that apply different allocation factors for a sectoral emission could be considered, for instance, the use of population density, only, for all sectoral emission studies.

(5) The CMAQ modeling with our emission data will be necessary to simulate the air pollutant concentration. Then the results could be compared with ground station or space-based observation to evaluate our results.

LIST OF REFERENCES

LIST OF REFERENCES

Akimoto, H (2003) Global Air Quality and Pollution, Science, 302, 1716-1719.

Akimoto, H. and H. Narita (1994), Distribution of SO_2, NOx, and CO_2 Emissions from Fuel Combustion and Industrial Activities in Asia with 1° × 1° Resolution, *Atmos. Environ.*, *28*, 213-225.

ACE-Asia, International Global Atmospheric Chemistry (IGAC) (2001), available at: http://saga.pmel.noaa.gov/Field/aceasia/ACEAsiaDescription.html

Beirle, S., U. Platt, M. Wenig, and T. Wagner (2003), Weekly Cycle of NO_2 By GOME Measurements: A Signature of Anthropogenic Sources, *Atmos. Chem. Phys.*, 3, 2225-2232.

California Air Researce Board (2002). Speciation tables provided by Mark Jacobson.

CAPSS (Clean Air Policy Support System): National Institute of Environmental Research (NIER), South Korea (2001)

China Electricity Statistical Yearbook 2005 (2006), p42 (In Chinese)

ESRI (Environmental Systems Research Institute) (1997), Digital Chart of the World (DCW) Data Description. Available at: http://data.geocomm.com/readme/dcw/dcw.html

Ethy, A., and K. Hanisak (2003), The MIMS Spatial Allocator: A Tool for Generating Emission Surrogates without a Geographic Information System. Available at http://www.epa.gov/ttn/chief/conference/ei12/modeling/eyth.pdf

Fu, J.S., D. G. Streets, C. J. Jang, J.M. Hao, K.B. He, L.T. Wang and Q. Zhang (2008). Modeling Regional/Urban Ozone and Particulate Matter in Beijing, China. *J. of Air and Waste Management Association*. (forthcoming)

Gery, M.W., G.Z. Whitten, J.P. Killus, and M.C. Dodge (1989), A Photochemical Kinetics Mechanism for Urban and Regional Scale Computer Modeling, *J. Geophys. Res.*, *94*, 925-956.

Heald, C. L., et al. (2003), Asian Outflow and Trans-Pacific Transport of Carbon Monoxide and Ozone Pollution: An Integrated Satellite, Aircraft, and Model Perspective, *J. Geophys. Res.*, *108(D24)*, 4804, doi: 10.1029/2003JD003507.

Hong Kong Environmental Protection Department (HKEPD), Study of Air Quality in the Pearl River Delta Region (Agreement No. CE 106/98) (2002), available at http://www.epd.gov.hk/epd/english/environmentinhk/air/studyrpts/study_pearl.html

Irie, H., K. Sudo, H. Akimoto, A. Richter, J. P. Burrows, T. Wagner, M. Wenig, S. Beirle, Y. Kondo, V. P. Sinyakov, and F. Goutail (2005), Evaluation of Long-Term Tropospheric NO_2 Data Obtained by GOME over East Asia in 1996-2002, *Geophys. Res. Lett.*, *32,* L11810, doi: 10.1029/2005GL022770.

Isukapalli, S. (1999), Uncertainty Analysis of Transport-Transformation Models, A dissertation submitted to the Graduate School--New Brunswick

Jaeglé, L., L. Steinberger, R. V. Martin and K. Chance (2005), Global Partitioning of NOx Sources Using Satellite Observations: Relative Roles of Fossil Fuel Combustion, Biomass Burning and Soil Emissions, *Faraday Discuss, 130*, 407-423.

Jian Dai and D. M. Rocke (2000), A GIS-Based Approach To Spatial Allocation of Area

Source Solvent Emissions, *Environmental Modelling & Software, 15*, 293-302

Kannari, A., Y. Tonooka, T. Baba, and K. Murano (2007) Development of multiple-species 1 km × 1 km resolution hourly basis emissions inventory for Japan, *Atmos. Environ., 41,* 3428–3439.

Kato, N. and H. Akimoto (1992), Anthropogenic Emissions of SO_2 and NOx in Asia: Emissions Inventories, *Atmos. Environ*., *26*, 2997-3017.

Kim, S.W., A. Heckel, S. A. McKeen, G. J. Frost, E.-Y. Hsie, M. K. Trainer, A. Richter, J. P. Burrows, S. E. Peckham, and G. A. Grell (2006), Satellite-Observed U.S. Power Plant NOx Emission Reductions and Their Impact on Air Quality, *Geophys. Res. Lett.*, *33*, L22812, doi: 10.1029/2006GL027749.

LandScan, Oak Ridge National Laboratory (2006), Available at http://www.ornl.gov/sci/landscan/landscanCommon/landscan_doc-main.html

Liu, S. H., X. B. Li, and M. Zhang (2003), Scenario Analysis on Urbanization and Rural - Urban Migration in China, Institute of Geographic Sciences and Natural Resources Research Chinese Academy of Sciences, Beijing.

Loveland, T.R., B.C. Reed, J.F. Brown, D.O. Ohlen, J. Zhu, L. Yang and J.W. Merchant (2000), Development of a Global Land Cover Characteristics Database and IGBP DISCover from 1-km AVHRR Data, *International Journal of Remote Sensing*, *21*, 6/7, 1303-1330.

Mark Z. Jacobson (2000). Fundamentals of Atmospheric Modeling. Cambridge University Press. pp. 656.

Martin, R. V., C. E. Sioris, K. Chance, T. B. Ryerson, T. H. Bertram, P. J. Wooldridge,

R. C. Cohen, J. A. Neuman, A. Swanson, and F. M. Flocke (2006), Evaluation of Space-Based Constraints on Global Nitrogen Oxide Emissions with Regional Aircraft Measurements Over and Downwind of Eastern North America, *J. Geophys. Res.*, *111* (D15308), doi: 10.1029/2005JD006680.

Martin, R. V., D. J. Jacob, K. Chance, T. P. Kurosu, P. I. Palmer, and M. J. Evans (2003), Global Inventory of Nitrogen Oxide Emissions Constrained by Space-Based Observations of NO_2 Columns, *J. Geophys. Res.*, *108*(D17), 4537, doi: 10.1029/2003JD003453.

Middleton, P. and W. R. Stockwell (1990). Arregation and Analysis of Volatile Organic Compound Emissions for Regional Modeling, *Atmos. Environ.*, *24A*, No.5, 1107-1133.

National Bureau of Statistics (NBS) (2007), China Statistical Yearbook 2006, China Statistics Press, Beijing (In Chinese)

Ohara, T., H. Akimoto, J. Kurokawa, N. Horii, K. Yamaji, X. Yan and T. Hayasaka (2007), An Asian Emission Inventory of Anthropogenic Emission Sources for the Period 1980-2020, *Atmos. Chem. Phys.*, *7*, 4419-4444

Olivier, J.G.J., A.F. Bouwman, C.W.M. Van der Maas, J.J.M. Berdowski, C. Veldt, J.P.J. Bloos, A.J.H. Visschedijk, P.Y.J. Zandveld and J.L. Haverlag (1996), Description of EDGAR Version 2.0. Rep. 771060 002, *Natl. Inst. Of Public Health and the Environ.* Bilthoven, Netherlands.

Olivier, J.G.J, J.P.J. Bloos, J.J.M. Berdowski, A.J.H. Visschedijk and A.F. Bouwman (1999), A 1990 Global Emission Inventory of Anthropogenic Sources of Carbon Monoxide on 1° × 1° Developed in the Framework of EDGAR/GEIA. *Chemosphere: Global Change Science*, *1*, 1-17.

Richter, A., P. Burrows, H. Nues, C. Granier and U. Niemeijer (2005), Increase in Tropospheric Nitrogen Dioxide Over China Observed from Space, *Nature*, *437*, 129-130.

Sexton, K. and J. Harvey (2002), Chamber Data for CB-IV Chemical Mechanism (SPMOD.xls), personal comunication with Ken Sexton

SMOKE (Sparse Matrix Operator Kernel Emissions) (2007), SMOKE v2.4 User's Manual. Available at http://www.smoke-model.org/version2.4/html/

Statistical Materials for Chinese Electrical Indutry (2006), 561-566 (In Chinese)

Stockwell, W. R., F. Kirchner and M. Kuhn (1997), A New Mechanism for Regional Atmospheric Chemistry Modeling. *J. Geophys. Res.*, *102* (D22), 25847-25879.

Streets, D.G., J. S. Fu, C. J. Jang, J. M. Haod, K. B. He, X. Y. Tang, Y. H. Zhang, Z.F. Wang, Z. P. Li, Q. Zhang, L. T. Wang, B. Y. Wang, and C. Yu (2007), Air Quality during the 2008 Beijing Olympic Games. *Atmosphric Environment 41*: 480–492

Streets, D. G., T. C. Bond, G. R. Carmichael, S. D. Fernandes, Q. Fu, D. He, Z. Klimont, S. M. Nelson, N. Y. Tsai, M. Q. Wang, J.-H. Woo, and K. F. Yarber (2003), An Inventory of Gaseous and Primary Aerosol Emissions in Asia in The Year 2000, *J. Geophys. Res.*, *108*, 8809, doi: 10.1029/2002JD003093.

Streets, D. G., Q. Zhang, L. Wang, K. He, J. Hao, Y. Wu, Y. Tang, and G. R. Carmichael (2006), Revisiting China's CO Emissions after the Transport and Chemical Evolution Over the Pacific (TRACE-P) Mission: Synthesis of Inventories, Atmospheric Modeling, and Observations, *J. Geophys. Res., 111*(D14306), doi: 10.1029/2006JD007118.

TRACE-P, National Aeronautics and Space Administration (NASA) (2001), available at: http://www-gte.larc.nasa.gov/gte_fld.htm#TRACE

UNCC (University of North Carolina Chapel Hill) (2003), MIMS Spatial Allocator User's Guide. Available at http://www.ie.unc.edu/cempd/projects/mims/spatial/

USEPA (United States Environmental Protection Agency) (1999), CMAQ Science Documentation. Available at: http://www.epa.gov/asmdnerl/CMAQ/CMAQscienceDoc.html

USGS (United States Geographical Survey) (2005), Global Land Cover Characteristics Data Base, Available at: http://edcsns17.cr.usgs.gov/glcc/globdoc2_0.html

Wang, L.T., J.M. Hao, K.B. He, S.X. Wang, J.H. Li, Q. Zhang, D. G. Streets, J. S. Fu, C. J. Jang, H. Takekawa and Satoru Chatani (2008). A Modeling Study of Coarse Particulate Matter Pollution in Beijing: Regional Source Contributions and Control Implications for the 2008 Summer Olympics. *J. of Air and Waste Management Association*, *58*:1057–1069.

Wang, X. P. D. L. Mauzeralla, Y.T. Hu, A.G. Russell, E.D. Larson, J.H. Wood, D.G. Streets and A. Guenther (2005), A High-Resolution Emission Inventory for Eastern China in 2000 and Three Scenarios for 2020, *Atmospheric Environment*, *39*, 5917-5933

Wang, Y. X., M. B. McElroy, T. Wang, and P. I. Palmer (2004), Asian emissions of CO and NOx: Constraints from aircraft and Chinese station data, *J. Geophys. Res.*, *109* (D24304), doi: 10.1029/2004JD005250.

Woo J.-H., J.M. Baek, J.-W. Kim, G.R. Carmichael, N. Thongboonchoo, S.T. Kim and

J.H. (2003), Development of a Multi-Resolution Emission Inventory and its Impact on Sulfur Distribution for Northeast Asia, *Water, Air and Soil Pollution, 148*, 259–327

Yarwood, G., S. Rao, M. Yocke, and G. Whitten (2005) Updates to the Carbon Bond Chemical Mechanism: CB05. Final Report to the US EPA, RT-0400675. Available at http://www.camx.com/publ/pdfs/CB05_Final_Report_120805.pdf.

Zhang, Q. et al. (2007), NOx Emission Trends for China, 1995-2004: the View from the Ground and the View from Space. *J. Geophys. Res., 112* (D14306), doi: 10.1029/2007JD008684.

Zhang, Q., D.G. Streets, K. He, S. Reddy, A. Kannari, I. Park, J.S.Fu and Z. Klimont (2007), A New Anthropogenic Emission Inventory System for Asia in Support of Atmospheric Modeling, *6th Annual CMAS Conference, Chapel Hill, NC*

Zhang, Q., D. G Streets, K.B. He and Z. Klimont (2007), Major Components of China's Anthropogenic Primary Particulate Emissions, *Environ. Res. Lett. 2*, 045027

Zhao, Y., et al. (2008), Primary Air Pollutant Emissions of Coal-Fired Power Plants in China: Current Status and Future Prediction, *Atmospheric Environment* doi:10.1016/j.atmosenv.2008.08.021

APPENDIX

Table 1 Coordinate system parameters for modeling domain

Parameter	Value
Projection	Lambert Conic Conformal
Alpha	15° N
Beta	40° N
x center	114° E
y center	28.5° N
False Southing	0
False Northing	0

Table 2 Horizontal domain settings for modeling domain

Domain	nx	ny	SW x (km)	SW y (km)	NE x (km)	NE y (km)
27-km (D1)	182	138	-2403	-1876.5	2511	1849.5
9-km (D2)	98	74	-522	-967.5	360	-301.5
3-km (D3)	152	110	-291	-754.5	165	-424.5
1-km (D4)	179	125	-103	-704.5	76	-579.5

Note: nx: number of grid cells in x direction; ny: number of grid cells in y direction; SW x: x value of southwest corner of the domain; SW y: y value of southwest corner of the domain; NE x: x value of northeast corner of the domain; NE y: y value of northeast corner of the domain.

Table 3 Vertical layer definitions for modeling domain

Layer	Sigma	Pressure (mb)	Height (m)	Depth (m)
25	0	50	20576	2419
24	0.285	321	8624	1029
23	0.4985	524	5135	652
22	0.641	659	3382	464
21	0.7229	737	2503	371
20	0.7937	804	1802	296
19	0.8251	834	1506	248
18	0.8521	859	1259	208
17	0.8753	882	1051	174
16	0.8951	900	877	146
15	0.912	916	730	122
14	0.9263	930	608	103
13	0.9385	942	505	86
12	0.9488	951	419	72
11	0.9575	960	346	61
10	0.9649	967	285	51
9	0.9711	973	234	43
8	0.9763	977	192	36
7	0.9807	982	156	30
6	0.9844	985	126	25
5	0.9875	988	101	23
4	0.9904	991	77	22
3	0.9931	993	55	20
2	0.9956	996	35	18
1	0.9979	998	17	17
0	1	1000	0	0

Table 4 Comparison between CB-IV and CB05 VOC species for Emission input to CMAQ model

CB-IV	Description	CB05	Description
ALD2	Higher aldehyde	ALD2	Acetaldehyde
		ALDX	Propionaldehyde and higher aldehydes
ETH	Ethene	ETH	Ethene
		ETHA	Ethane
		ETOH	Ethanol
		MEOH	Methanol
FORM	Formaldehyde	FORM	Formaldehyde
OLE	Olefinic carbon bond	OLE	Terminal olefin carbon bond (R-C=C)
		IOLE	Internal olefin carbon bond (R-C=C-R)
		NASN	N/A
PAR	Paraffin carbon bond	PAR	Paraffin carbon bond (C-C)
ISOP	Isoprene	ISOP	Isoprene
TERPB	Terpene	TERP	Terpene
TOL	Toluene	TOL	Toluene and other monoalkyl aromatics
NR	Non reactive	NR	Non reactive
XYL	Xylene	XYL	Xylene and other polyalkyl aromatics

Note: species in red color are new species only exist in CB05. [Gery et al., 1989; Yarwood, 2005]

Table 5 USGS Land Use/Land Cover (LULC) System Legend

Type ID	Description
1	Urban and Built-Up Land
2	Dryland Cropland and Pasture
3	Irrigated Cropland and Pasture
5	Cropland/Grassland Mosaic
6	Cropland/Woodland Mosaic
7	Grassland
8	Shrubland
10	Savanna
11	Deciduous Broadleaf Forest
12	Deciduous Needleleaf Forest
13	Evergreen Broadleaf Forest
14	Evergreen Needleleaf Forest
15	Mixed Forest
16	Water Bodies
17	Herbaceous Wetland
18	Wooded Wetland
19	Barren or Sparsely Vegetated
20	Herbaceous Tundra
21	Wooded Tundra
22	Mixed Tundra
23	Bare Ground Tundra
24	Snow or Ice
100	Missing Data

Table 6 Mapping Table from TRACE-P to CB05 w/ $PM_{2.5}$ speciation

TRACE-P			Mapping from TRACE-P to CB05	CB05 w/ $PM_{2.5}$
No	Species	MW		Species
1	Ethane	30.0	0.5*[16]	ALD2
2	Propane	44.0	[16]	ALDX
3	Butanes	58.0	[6]	ETH
4	Pentanes	72.0	[1]	ETHA
5	Other Alkanes	86.0	N/A	ETOH
6	Ethene	28.0	[15]	FORM
7	Propene	40.0	[9]	IOLE
8	Terminal Alkenes	56.2	[30]	ISOP
9	Internal Alkenes	56.2	N/A	MEOH
10	Acetylene	26.0	N/A	NASN/NVOL
11	Benzene	78.0	[7]+[8]+0.5*[32]	OLE
12	Toluene	92.0	1.5*[2]+4*[3]+5*[4]+6*[5]+1*[7]+2*[8]+[10]+[11]+[16]+8*[17]+1.33*[19]+8.5*[32]	PAR
13	Xylenes	106.0	[31]	TERP
14	Other Aromatics	117.0	[12]+0.5*[14]	TOL
15	HCHO	30.0	1.5*[2]+[10]+5*[11]+[24]+0.5*[32]	UNR
16	Other Aldehydes	88.0	[13]+0.5*[14]	XYL
17	Ketones	126.0	0.9*[21]	NO
18	Halocarbons	150.0	0.1*[21]	NO2
19	Other	72.0	[25]	PEC
20	SO_2	64.0	[29]-[28]	PMC
21	NOx	46.0	[28]-[25]-[26]-PNO3-PSO4	PMFINE
22	CO2	44.0	[28]*x	PNO3
23	CO	28.0	[26]	POA
24	CH_4	16.0	[28]*x	PSO4
25	BC	12.0	[20]	SO_2
26	OC	12.0	0.02*[20]	SULF
27	NH_3	17.0	[23]	CO
28	$PM_{2.5}$		[27]	NH_3
29	PM_{10}		[24]	CH_4
30	ISOP (biogenic,GEIA)	5 carbons	[22]	CO_2

Table 6 (Cont.)

Trace-P			Mapping from TRACE-P to CBO5	CB05 w/ $PM_{2.5}$
31	TERP (biogenic,GEIA)	10 carbons		
32	Other VOC (biogenic,GEIA)	10 carbons		

Note: Number in square brackets is the TRACE-P species Number (NO.) x value is sector dependent. Please refer to Table 7. [Fu et al., 2008]

Table 7 x values to split PM mass in each sector

Sector	PNO3	PSO4
Power plant	0	0
Industrial	0	0.119
Transport	0.00395	0.0187
Domestic	0	0
Livestock	0.0011	0.0004
Biomass Burning	0	0.068

Note: The x values is from Fu et al., 2008

Table 8 Allocation factors Reference Table (All species except NH_3 and CH_4)

Emission Source Type	Emission sector	AF Type	Source
Point	LPS	AF_LPS	large power plants
Line	Transportation	AF_rd	road network
	Ship	AF_ship	shiplane
Area	Resdential	AF_pop	population
	Industry	AF_urban	urban population
	POWS	AF_pop	population

Table 9 Allocation factors Reference Table (NH_3 and CH_4)

CH_4	AF	NH_3	AF
Rice Cultivation	AF_crop	Cattle	AF_rural
Animal Emissions	AF_rural	Pigs	AF_rural
Landfills	AF_urban	Other Animals	AF_rural
Wastewater Treatment	AF_urban	Fertilizer Use	AF_crop
Coal Mining and Combustion	AF_pop	Biofuel Use	AF_rural
Oil and Gas Extraction and Use	AF_urban	Other Sources	AF_pop
Biofuel Combustion	AF_rural		

Note: AF_crop- Allocation factors generated from crop landcover which responses to the LULC category ID 2, 5 and 6 (See Table 4).

Table 10 Sectoral Emission Vertical distributions

Vertical Layer	Height (m)	Sector
1	17	[Resd]+[Tra]+ [Pows]+[Ship]+[Livst]+[Biog]
2	35	[Ind]+[BB]
3	55	0.00
4	77	0.00
5	101	0.00
6	126	0.00
7	156	0.1*[LPS]
8	192	0.4*[LPS]
9	234	0.45*[LPS]
10	285	0.05*[LPS]
11 ~ 25	285 ~ 20576	0.00

Note: Resd: Residential; Tra-Transportation; Pows: small power plants; Livst-livestaock: Biog: biogenic; Ind: industry; BB: biomass burning; LPS: large point souces.
The ratio is simply interpolated with the layer height based on the 14 vertical layers set in CMAQ modeling for Beijing Olympic Games [Streets and Fu et al., 2007]

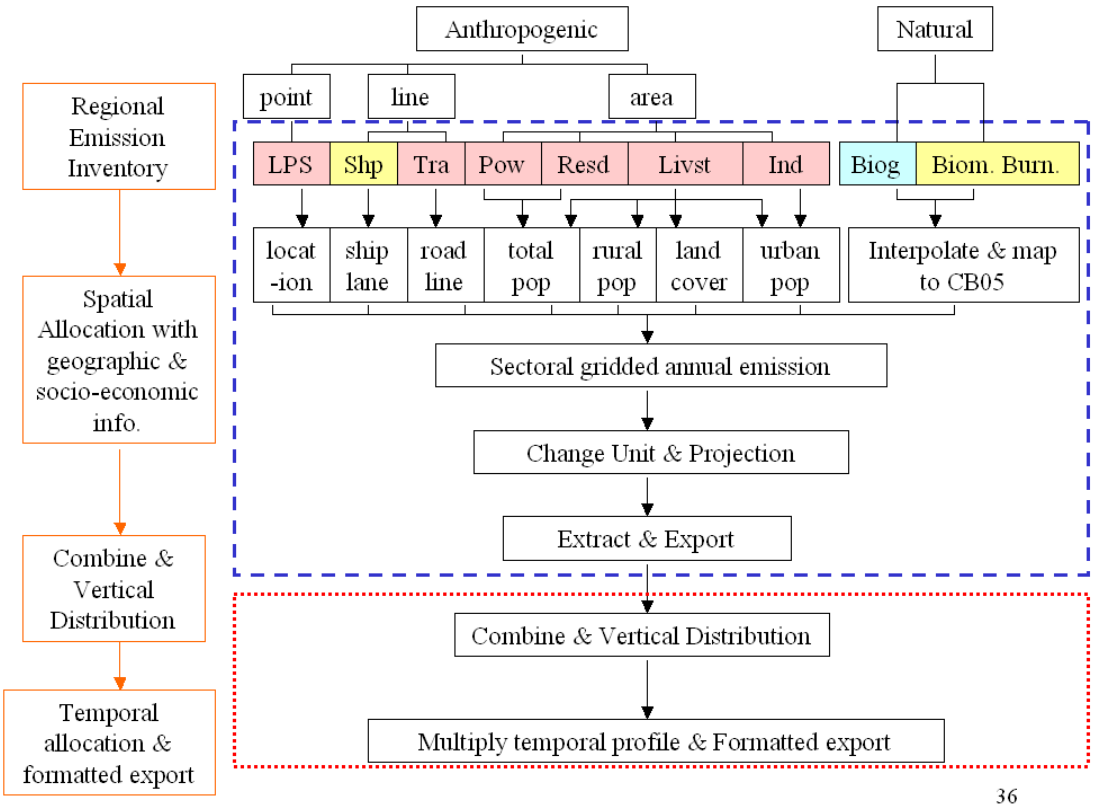

Flow Chart of Emission Process

Note:
Blue dash box: GIS program;
Red dot box: FORTRAN program.
Pink shadow: from INTEX-B emission inventory;
Yellow shadow: from TRACE-P emission inventory;
Blue shadow: from GEIA

Figure 1 Flow Chart

(a)

(b)

Figure 2 Domains overview: (a) Asia; (b) Four modeling domains

Unit: Gg of SO_2 Year: 2006	Power	Industry	Residential	Transportation	Total
Anhui	337.3	280.9	69.5	5.1	692.8
Beijing	118.0	62.0	62.7	4.9	247.6
Chongqing	588.9	447.1	173.8	1.4	1211.2
Fujian	263.0	172.3	22.2	2.9	460.4
Zhejiang	648.4	759.7	19.3	6.7	1434.1
China Total	**18333.4**	**9725.1**	**2837.7**	**123.3**	**31019.5**
Japan	142.0	475.5	65.0	188.7	871.1
Korea, Rep of	95.1	294.8	42.3	64.3	496.6
Korea, DPR	45.1	162.8	22.0	3.5	233.4
Mongolia	48.6	31.2	3.3	0.5	83.5
Taiwan, China	159.8	21.4	0.7	7.2	189.1
Other East Asia Total	**490.7**	**985.7**	**133.2**	**264.1**	**1873.7**
Brunei	2.5	1.1	0.8	2.7	7.1
Cambodia	7.0	13.7	7.6	6.1	34.3
Indonesia	409.1	566.8	193.2	291.7	1450.7
Laos	0.0	2.6	2.4	2.9	7.8
Malaysia	824.4	274.5	9.8	28.0	1136.6
Myanmar	0.6	19.1	29.5	1.9	51.1
Philippines	296.3	548.0	77.4	21.8	943.5
Singapore	134.8	17.8	6.9	3.9	163.4
Thailand	466.4	775.6	27.1	30.3	1299.4
Vietnam	57.9	210.0	94.8	22.6	385.3
Southeast Asia Total	**2198.8**	**2419.2**	**449.4**	**411.9**	**5479.2**
Bangladesh	20.2	36.2	61.1	30.6	148.1
Bhutan	0.1	3.0	1.5	0.8	5.3
India	2581.0	2282.0	349.3	383.2	5595.5
Nepal	0.8	5.9	21.5	2.9	31.1
Pakistan	421.3	2179.8	70.1	210.7	2881.9
Sri Lanka	5.4	51.6	21.5	20.0	98.5
South Asia Total	**3028.7**	**4558.5**	**525.0**	**648.2**	**8760.3**
Asia Total	**24051.5**	**17688.5**	**3945.3**	**1447.4**	**47132.8**

(a)

Unit: Gg of NH_3 Year: 2006	Cattle	Pigs	Other Animals	Fertilizer Use	Biofuel Use	Other Sources	Total
Anhui	58.9	85.4	37.2	417.2	22.6	40.6	661.9
Beijing	1.9	13.8	11.3	28.0	2.1	8.3	65.3
Chongqing							0.0
Fujian	11.0	60.1	19.0	203.2	15.8	22.0	331.1
Gansu	34.6	37.5	40.2	68.0	9.6	15.5	205.4
China Total	**1205.6**	**2409.4**	**1427.0**	**6883.8**	**601.6**	**816.2**	**13343.7**
Japan	91.9	49.3	79.3	45.3	5.1	77.7	348.7
Korea, Rep of	37.4	35.6	19.6	46.9	1.5	28.9	169.9
Korea, DPR	5.3	7.7	4.2	39.9	23.9	14.5	95.6
Mongolia	44.3	0.1	68.2	0.1	2.4	2.0	117.1
Taiwan, China	19.3	43.3	9.8	65.6	0.4	13.0	151.4
Other East Asia Total	**198.2**	**136.0**	**181.1**	**197.8**	**33.3**	**136.2**	**882.7**
Brunei	0.0	0.0	1.3	0.5	0.1	0.2	2.2
Cambodia	34.6	14.3	4.5	0.8	8.3	7.1	69.6
Indonesia	139.5	51.5	221.7	548.1	177.0	134.8	1272.6
Laos	11.4	6.1	3.7	0.2	2.8	3.4	27.5
Malaysia	8.3	10.1	32.4	43.4	7.1	14.6	115.9
Myanmar	126.4	21.6	14.8	41.4	28.6	29.0	261.8
Philippines	29.4	57.3	44.5	42.5	20.3	48.2	242.2
Singapore	0.0	1.0	0.6	0.1	0.0	2.5	4.3
Thailand	70.3	42.3	47.0	93.8	24.9	39.8	318.2
Vietnam	47.7	111.2	62.7	299.8	73.6	50.7	645.6
Southeast Asia Total	**467.7**	**315.3**	**433.3**	**1070.6**	**342.8**	**330.4**	**2960.0**
Bangladesh	272.7	0.0	63.6	270.8	48.4	81.8	737.3
Bhutan	5.0	0.4	0.6	0.0	1.6	1.3	9.0
India	2522.3	90.9	269.4	3164.2	546.9	635.7	7229.3
Nepal	81.0	5.0	10.1	26.7	21.3	14.4	158.6
Pakistan	253.6	0.0	150.7	626.5	78.8	86.7	1196.3
Sri Lanka	18.6	0.4	2.9	43.6	8.3	12.3	86.1
South Asia Total	**3153.2**	**96.6**	**497.4**	**4131.9**	**705.3**	**832.2**	**9416.7**
Asia Total	**5024.7**	**2957.4**	**2538.8**	**12284.1**	**1683.0**	**2115.0**	**26603.0**

(b)

Figure 3 INTEX-B 2006 regional emission inventory samples: (a) SO_2; (b) NH_3

(From: Zhang et al, 2007, available at:
http://www.cgrer.uiowa.edu/EMISSION_DATA_new/index_16.html)

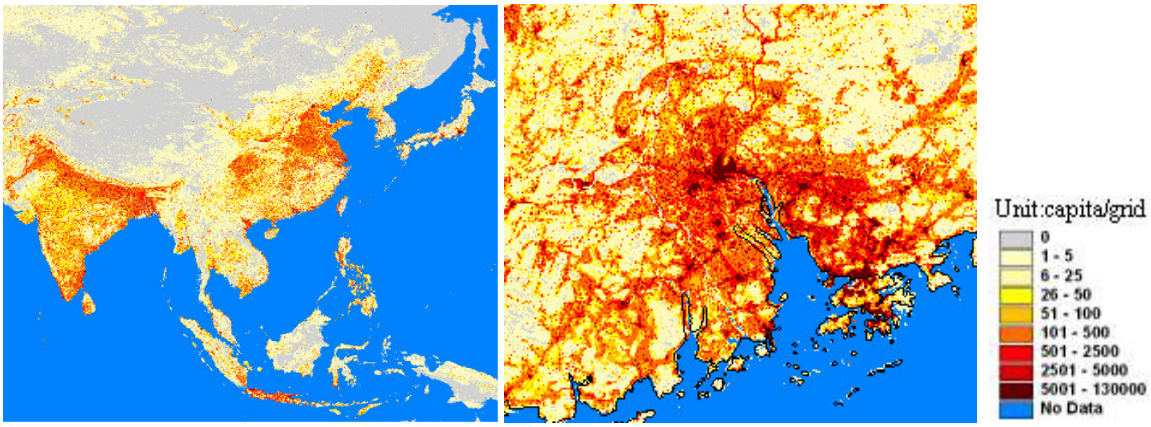

(a) (b)

Figure 4 LandScan 2006 Population distribution

(a) Asia; (b) Pearl River Delta (PRD) Region (From: LandScan 2006)

Figure 5 Road Network

(From: Chinese Consulting agencies and DCW)

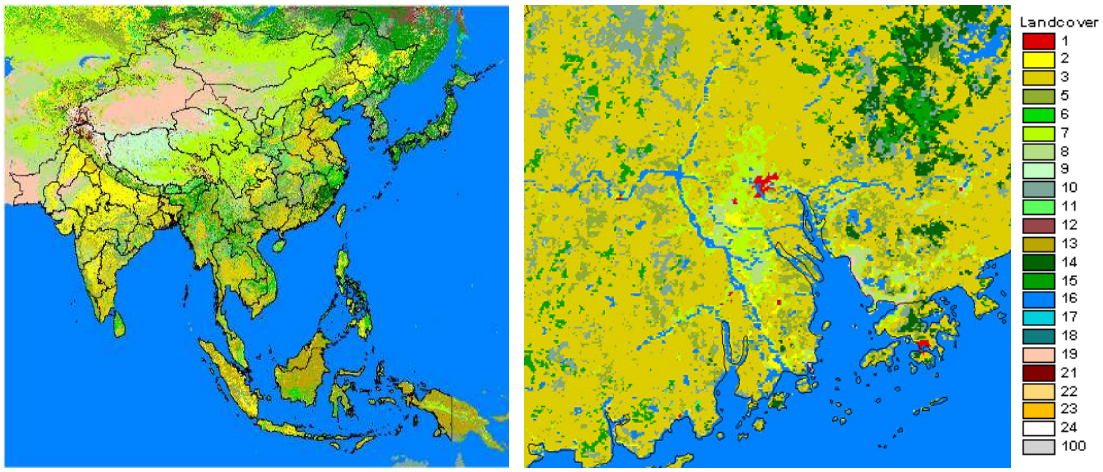

(a) (b)

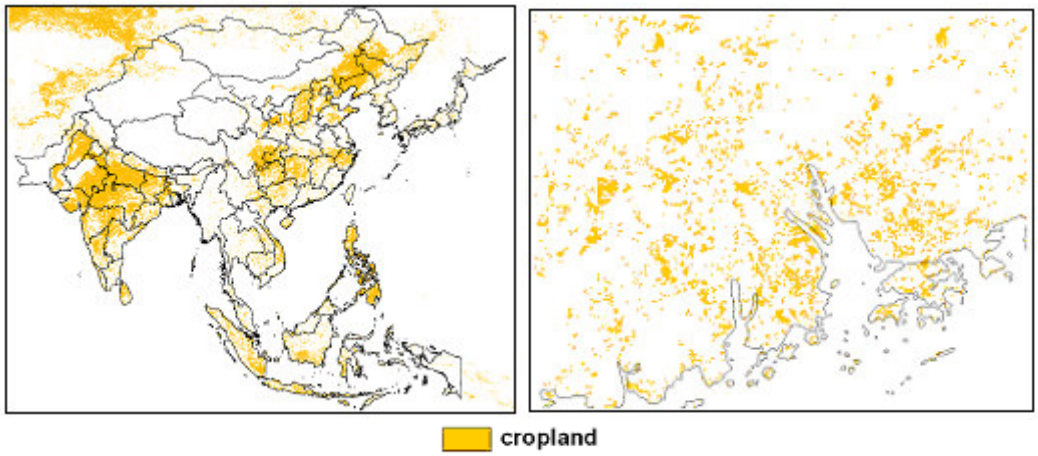

(c) (d)

Figure 6 (a) Land Cover in Asia; (b) Land Cover in PRD region; (c) Cropland cover for Asia; (d) Cropland cover in PRD region

(From: Global Land Cover Characteristics Database, available at: http://edcsns17.cr.usgs.gov/glcc/globe_int.html)

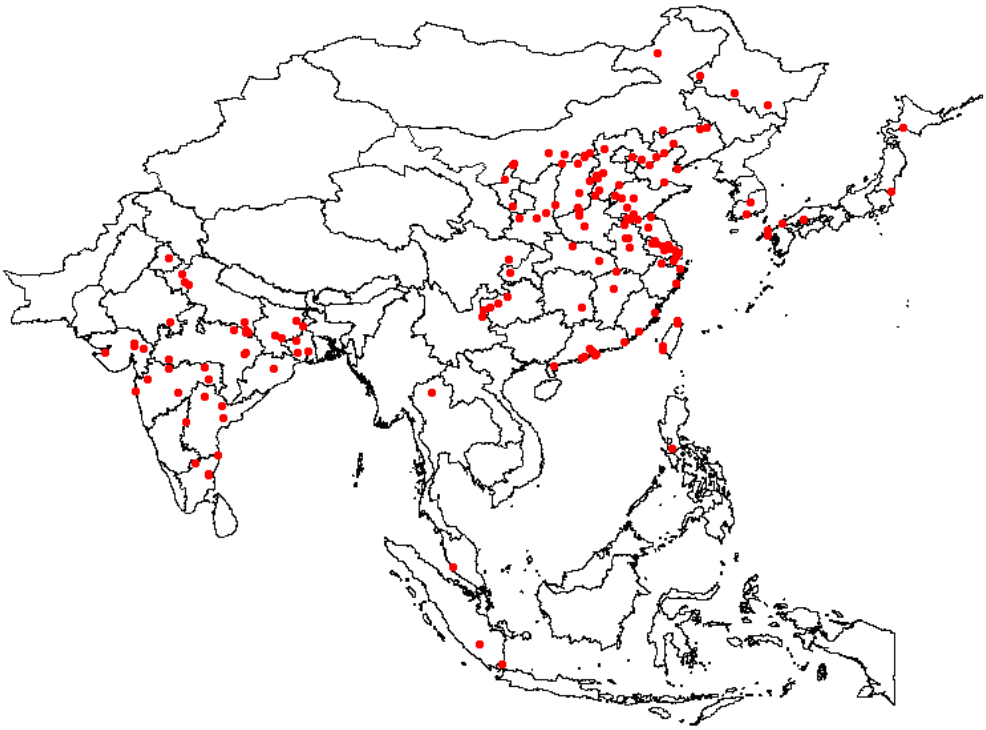

Figure 7 Large Point Sources Distribution

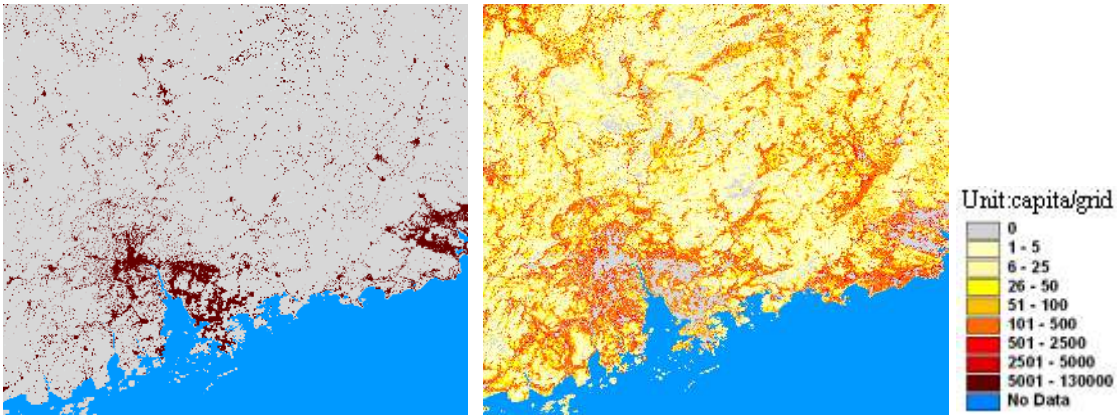

(a) (b)

Figure 8 Mapping urban/rural population: (a) urban population; (b) rural population

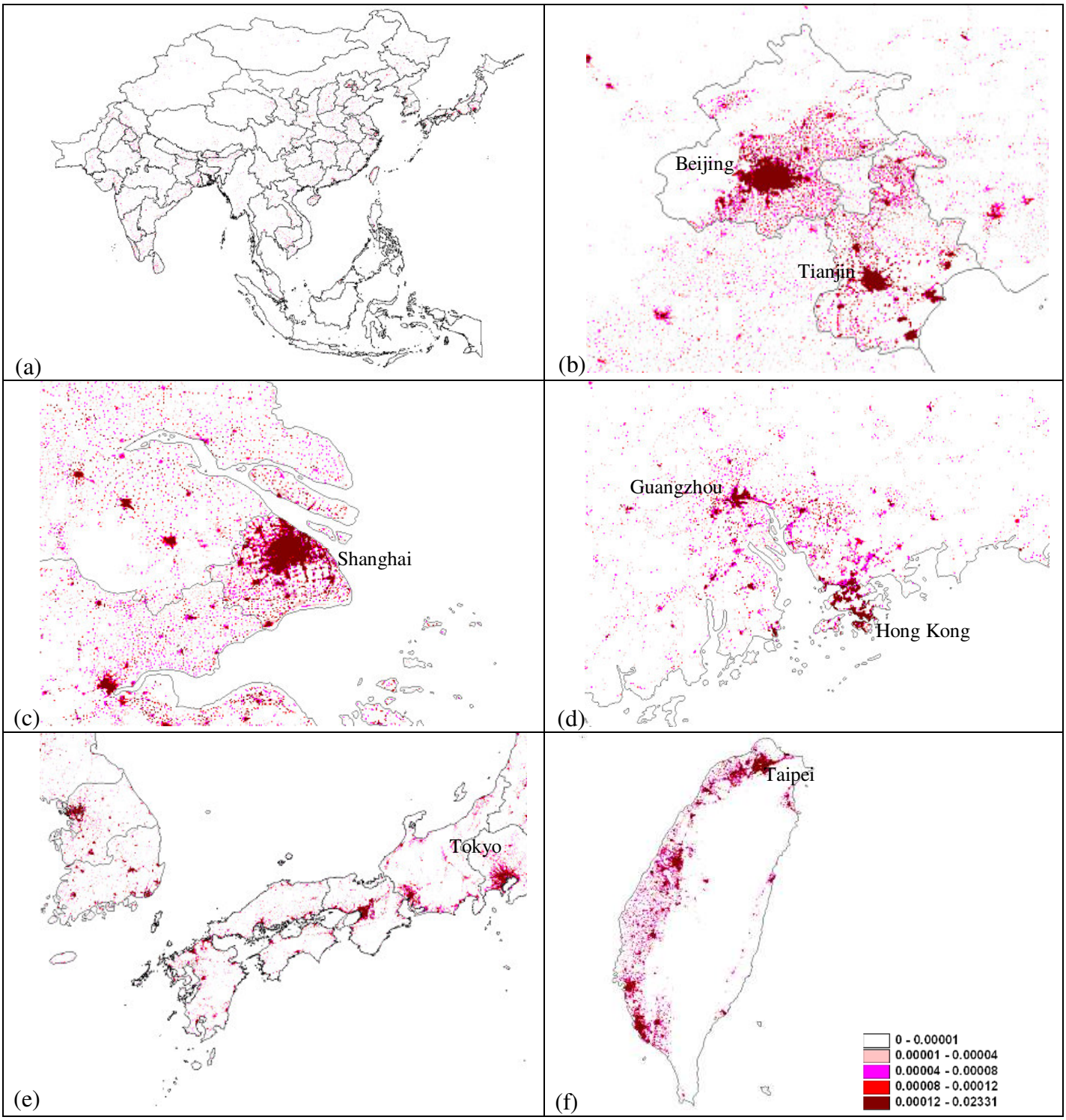

Figure 9 AF_pop: (a) Asia; (b) Beijing & Tianjin; (c) Shanghai; (d) PRD region; (e) Japan; (f) Taiwan

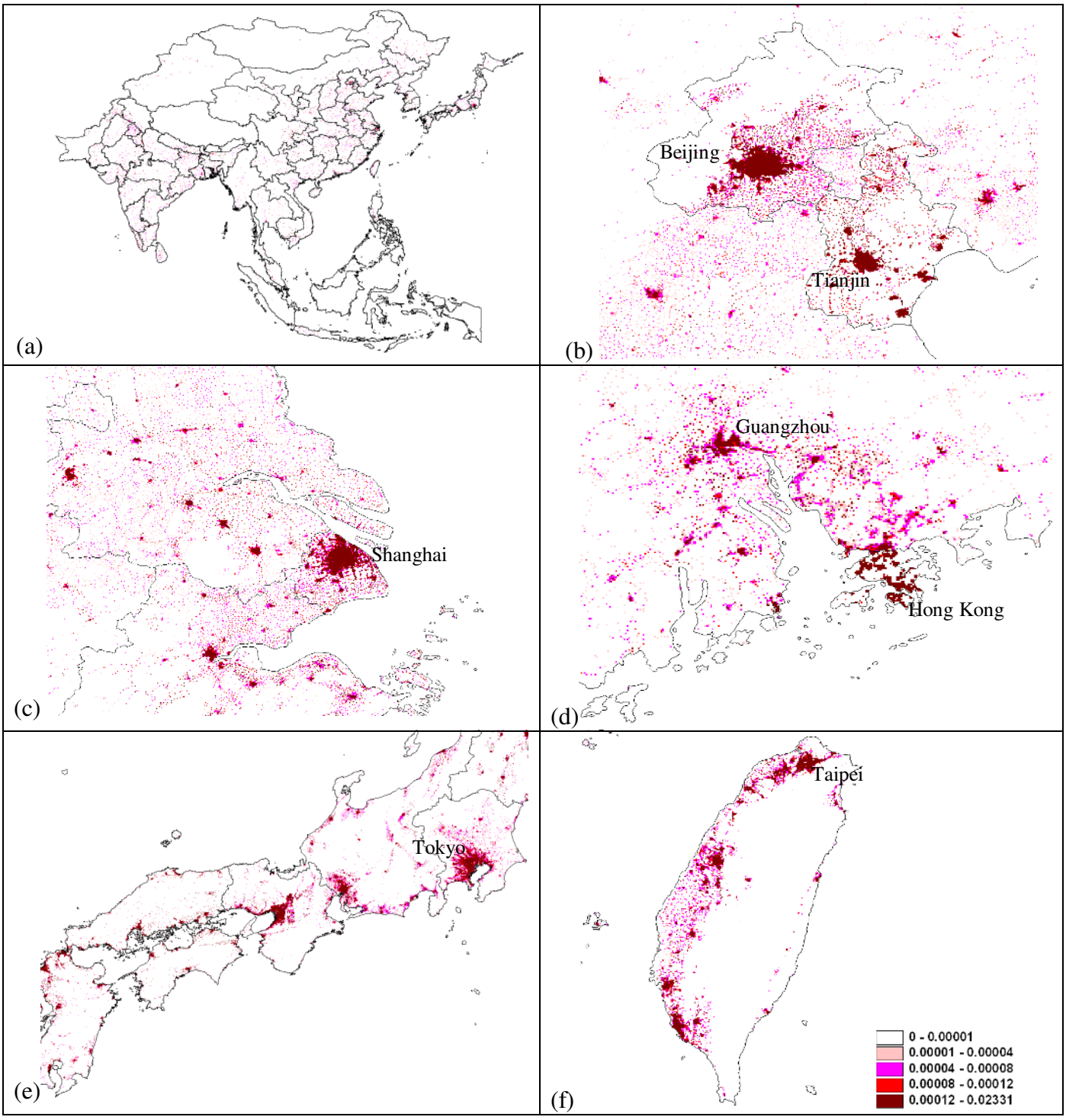

Figure 10 AF_urban: (a) Asia; (b) Beijing & Tianjin; (c) Shanghai; (d) PRD region; (e) Japan; (f) Taiwan

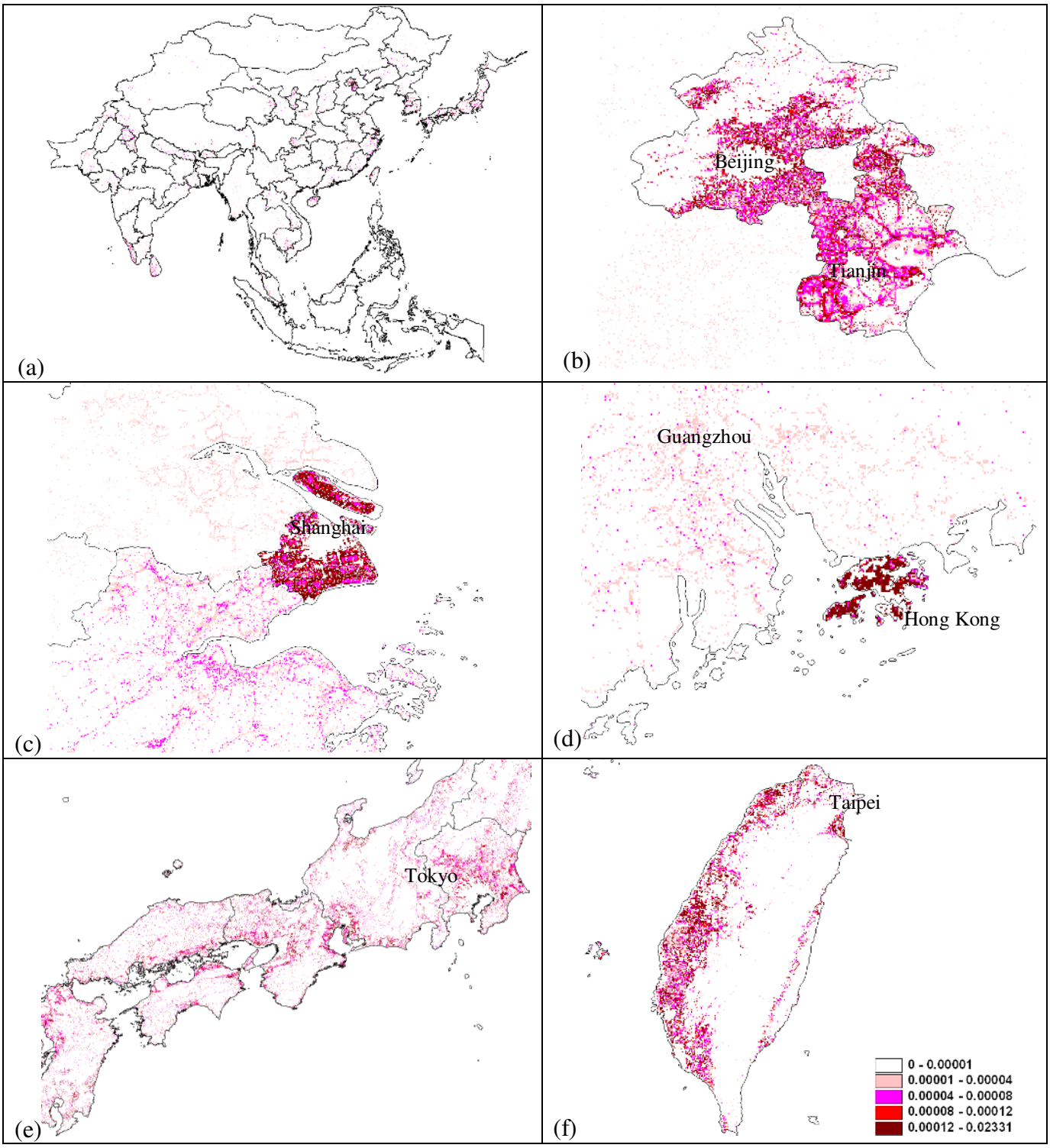

Figure 11 AF_rural: (a) Asia; (b) Beijing & Tianjin; (c) Shanghai; (d) PRD region; (e) Japan; (f) Taiwan

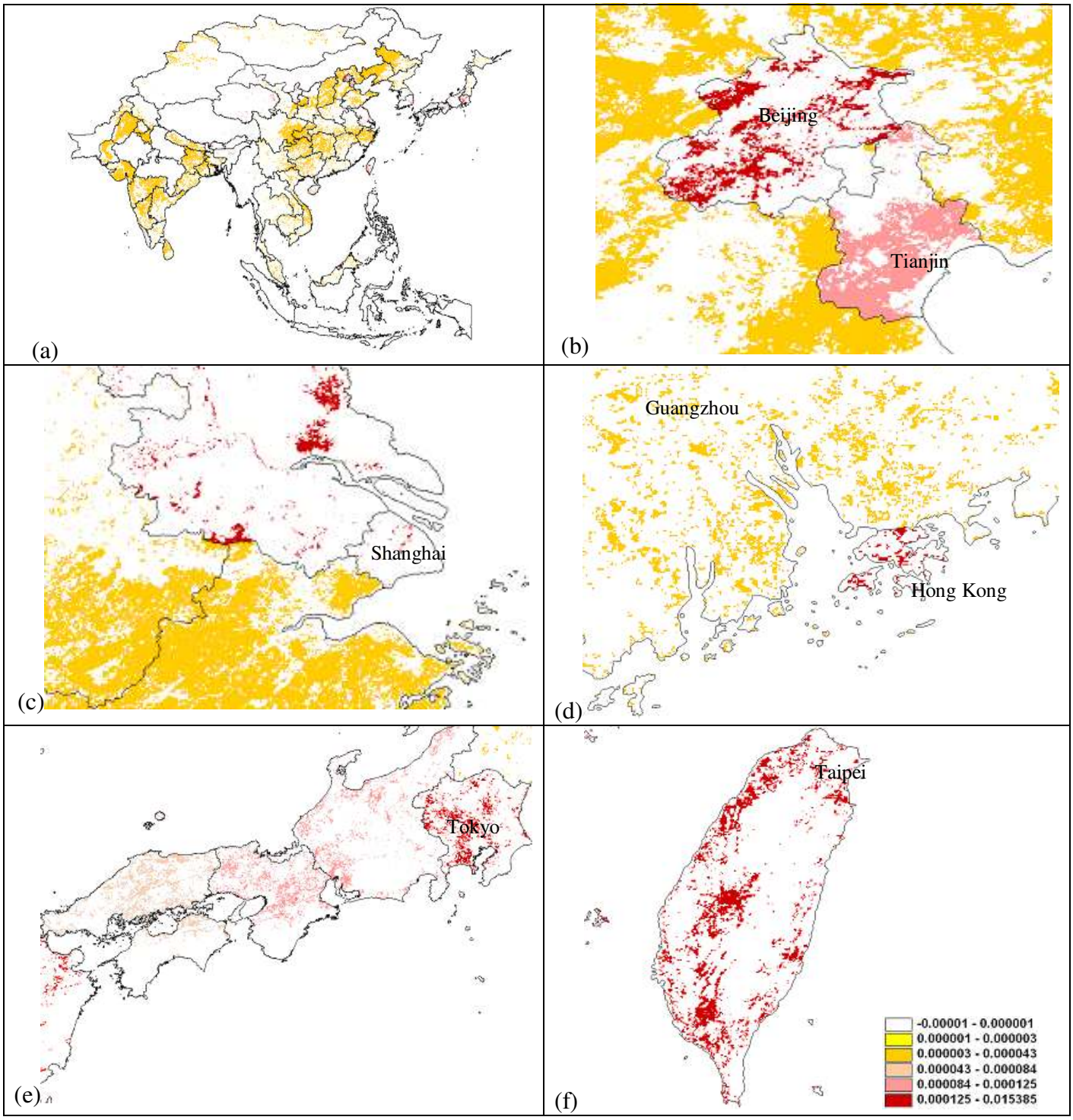

Figure 12 AF_crop: (a) Asia; (b) Beijing & Tianjin; (c) Shanghai; (d) PRD region; (e) Japan; (f) Taiwan

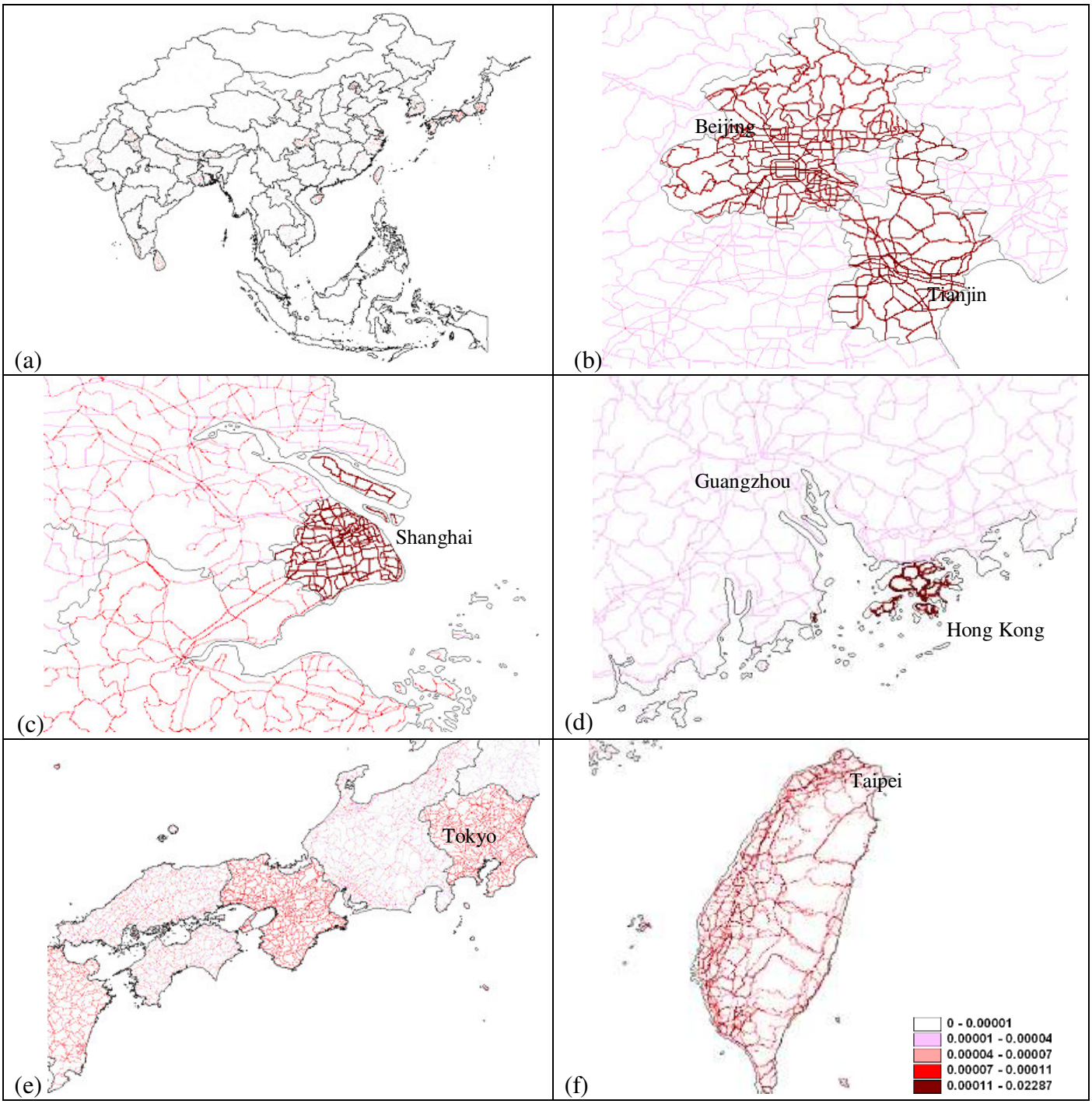

Figure 13 AF_rd: (a) Asia; (b) Beijing & Tianjin; (c) Shanghai; (d) PRD region; (e) Japan; (f) Taiwan

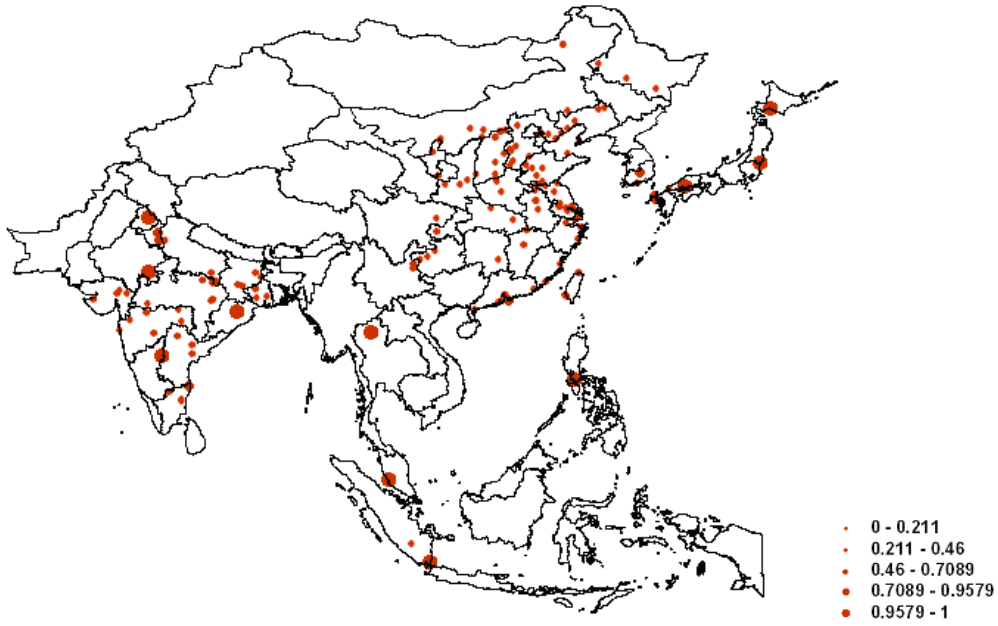

Figure 14 AF_LPS

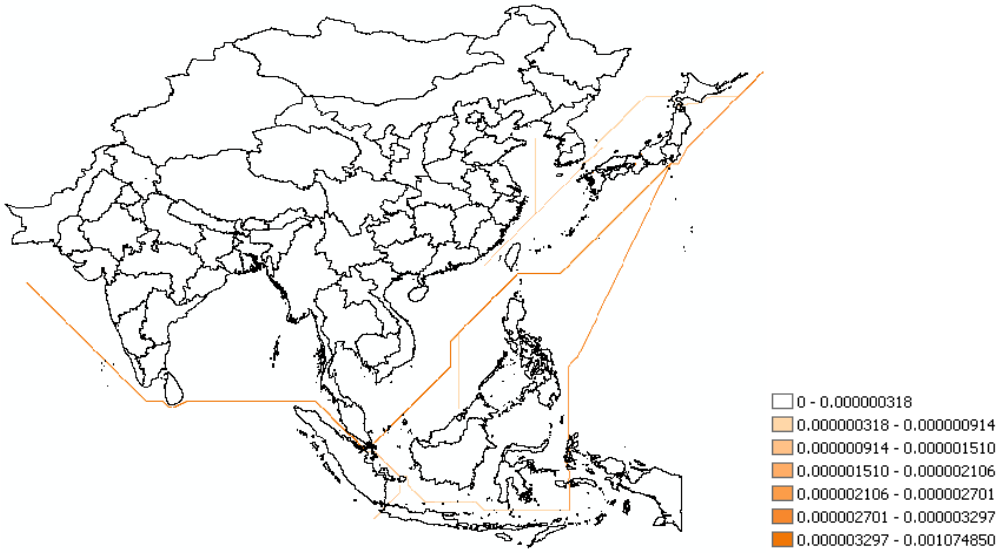

Figure 15 AF_ship

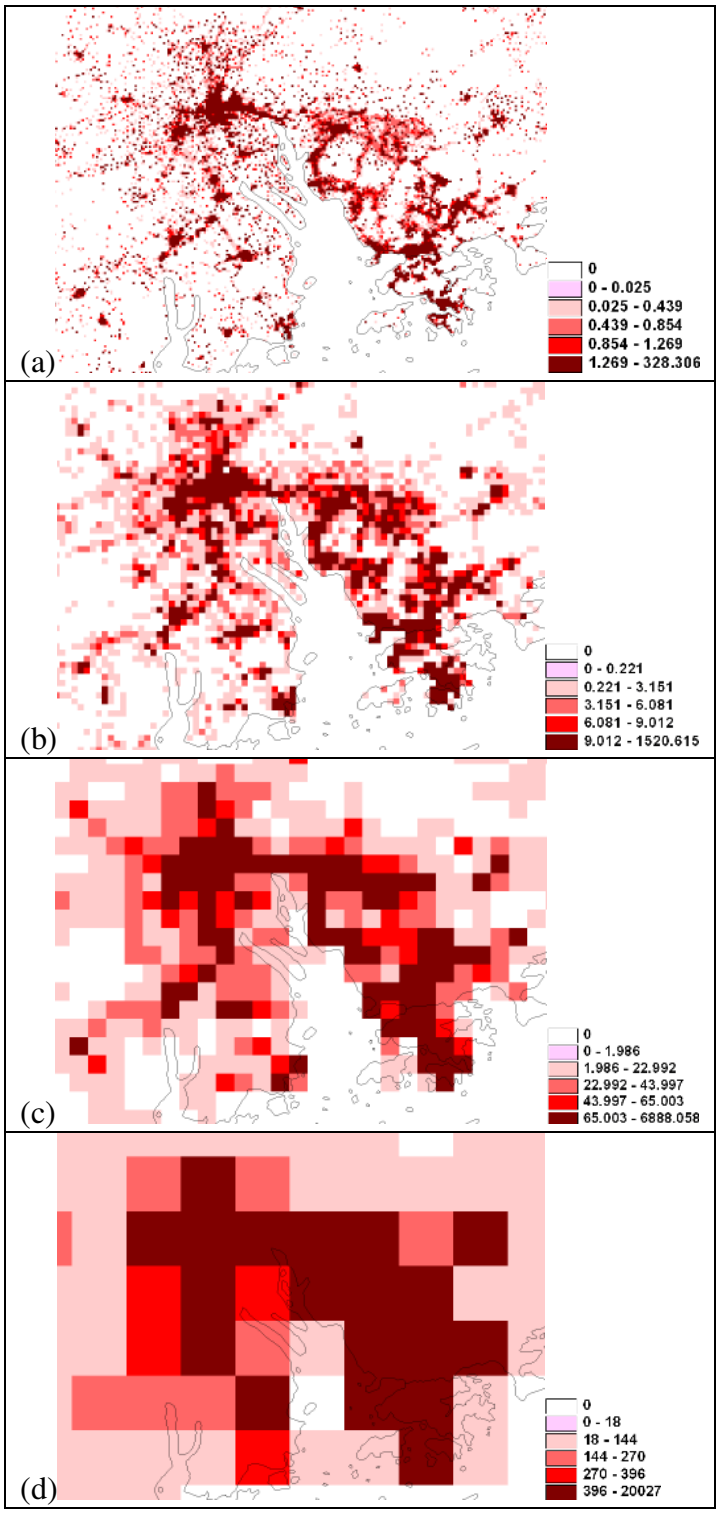

Figure 16 Residential NOx emission in PRD region aggregation in resolution of: (a) 0.5min; (b) 1.5min; (c) 4.5min; (d) 13.5min

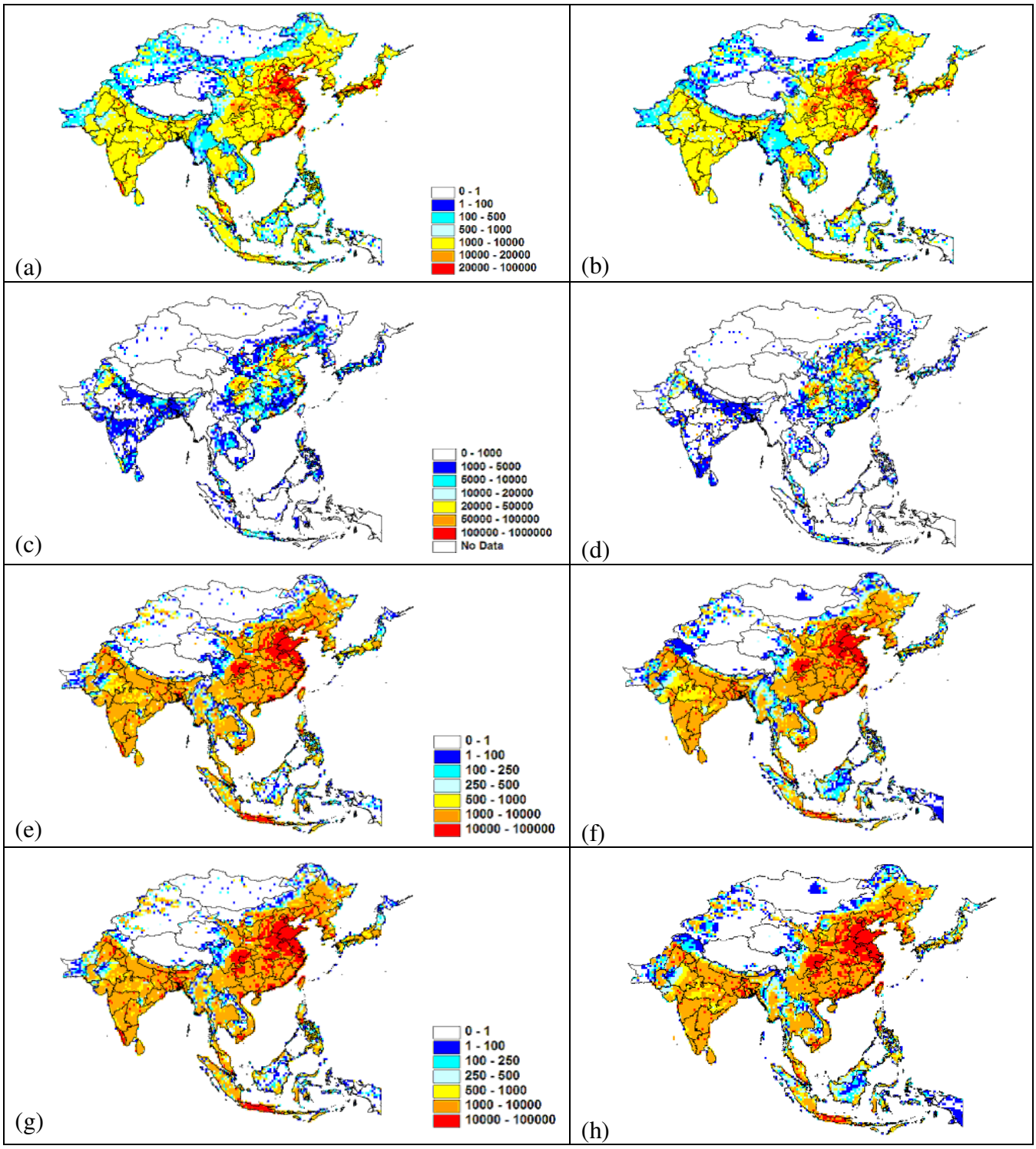

Figure 17 Our gridded annual emission (left) vs. INTEX-B (right) in resolution of 0.5° × 0.5° (~55km × 55km): (a) ~ (b): NOx; (c) ~ (d): SO_2; (e) ~ (f): $PM_{2.5}$; (g) ~ (h): PM_{10} (Unit: ton/yr/grid)

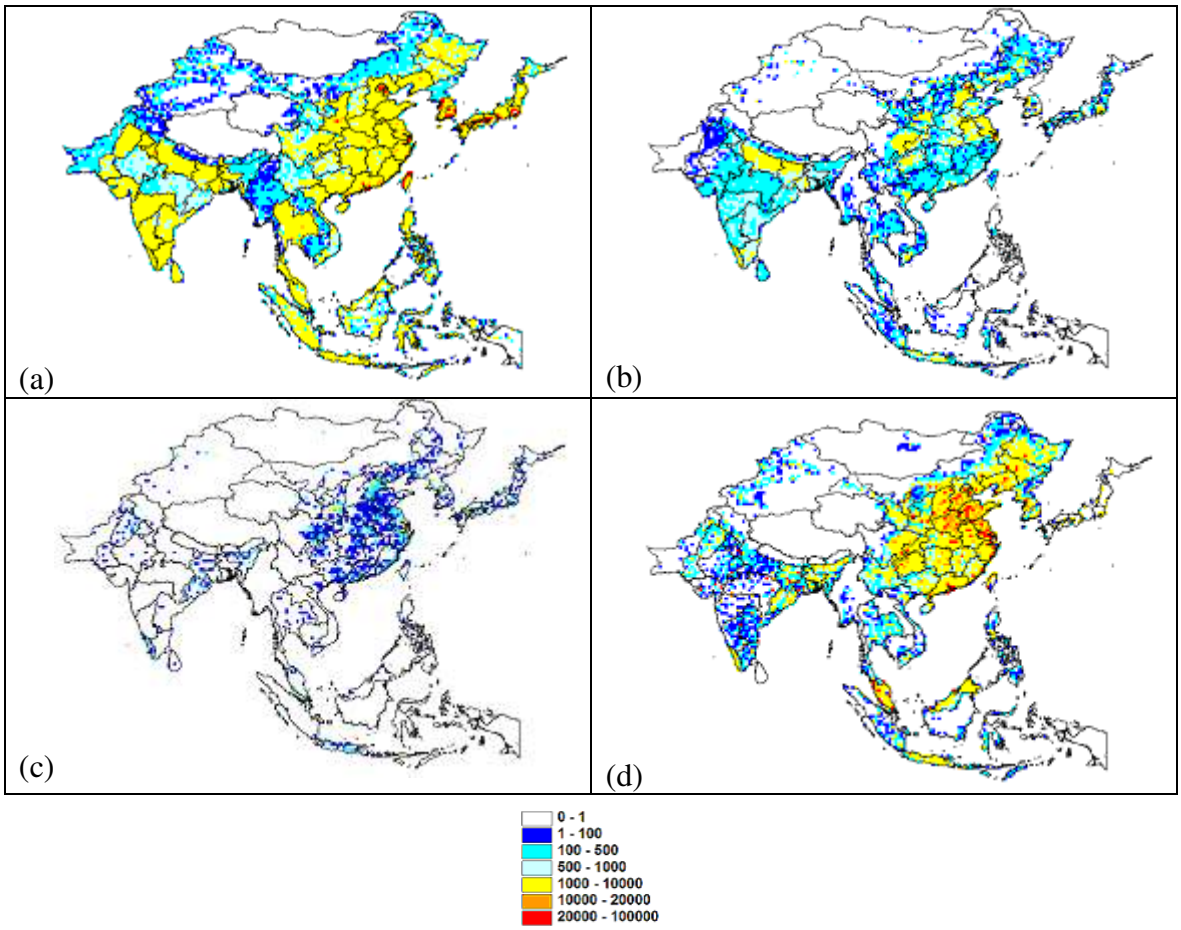

Figure 18 INTEX-B sectoral NOx emissions in resolution of 0.5° × 0.5° (~55km × 55km): (a) Transportation; (b) residential; (c) Industry; (d) Power (Unit: ton/yr/grid)

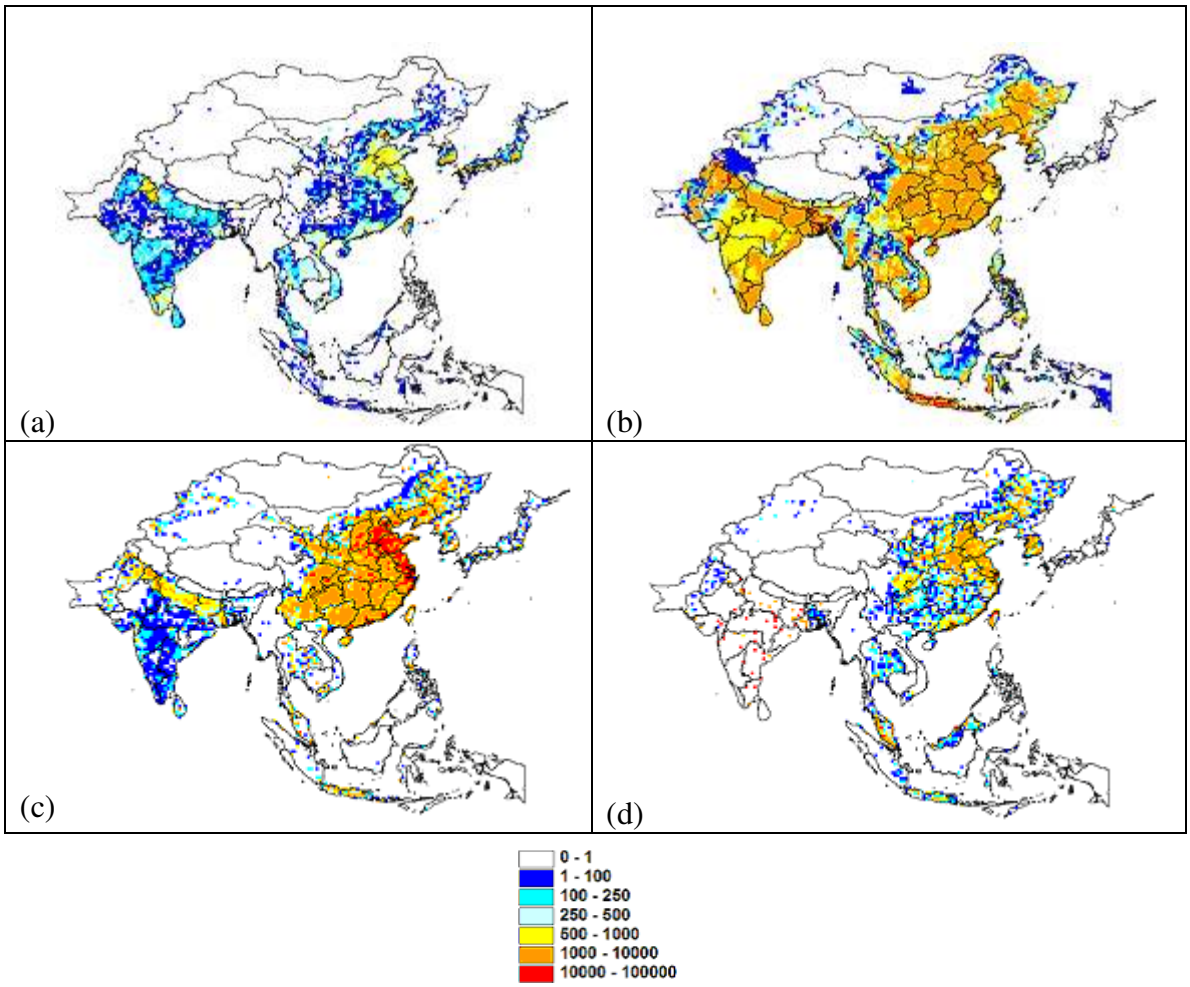

Figure 19 INTEX-B sectoral $PM_{2.5}$ emissions in resolution of 0.5° × 0.5° (~55km × 55km): (a) Transportation; (b) residential; (c) Industry; (d) Power (Unit: ton/yr/grid)

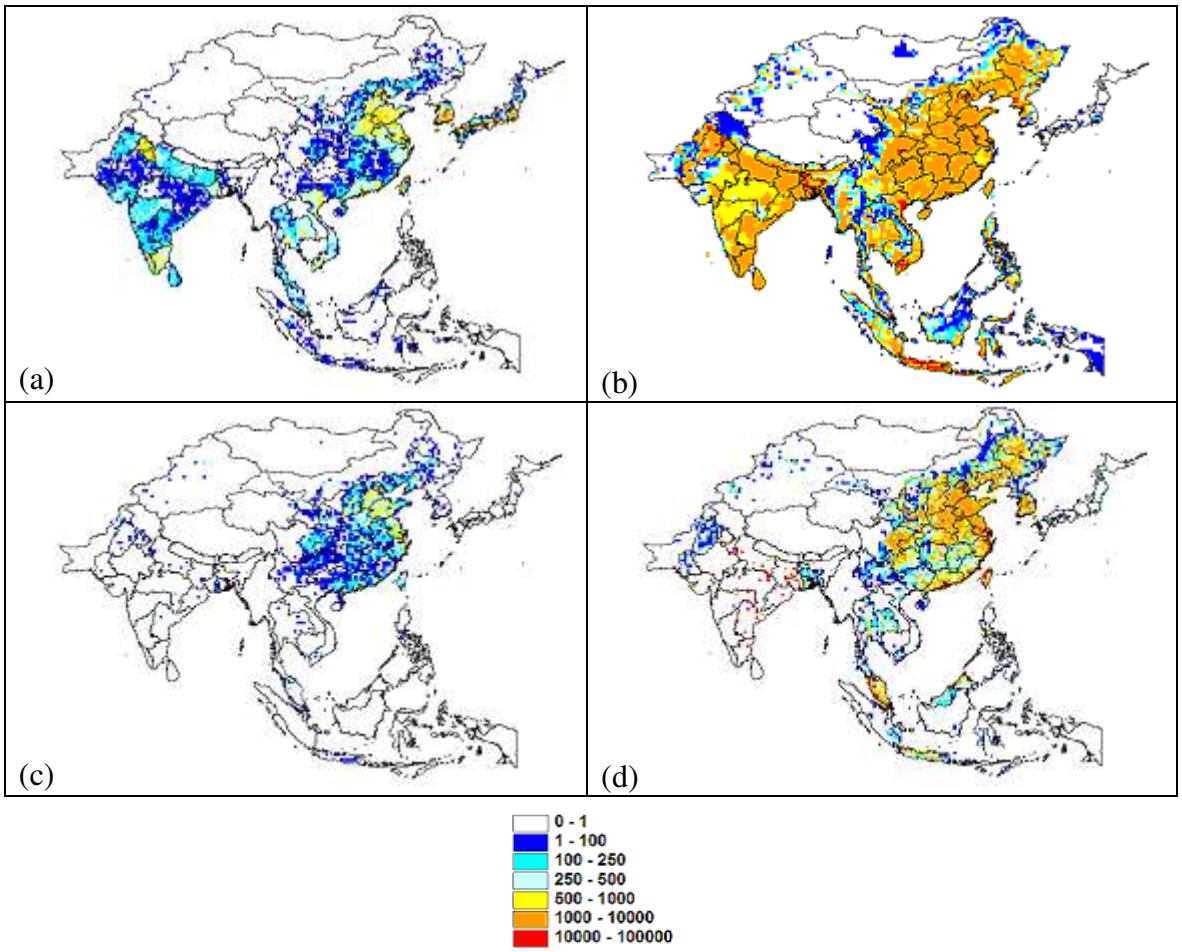

Figure 20 INTEX-B sectoral PM_{10} emissions in resolution of 0.5° × 0.5° (~55km × 55km): (a) Transportation; (b) residential; (c) Industry; (d) Power (Unit: ton/yr/grid)

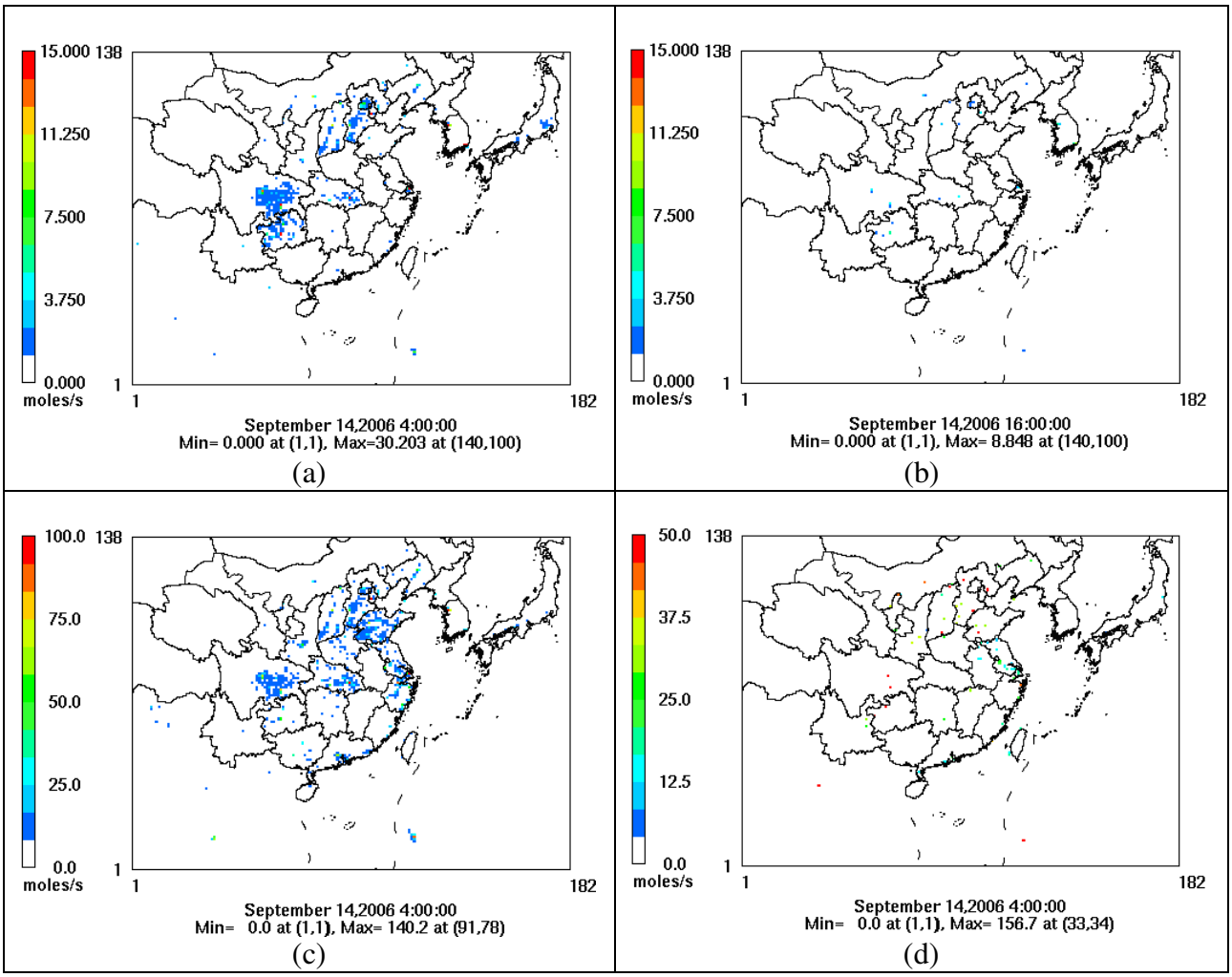

Figure 21 SO_2 emission in 27km × 27km domain 1: (a) layer 1 at 12:00; (b) layer 1 at 24:00; (c) layer 2 at 12:00; (d) layer 9 at 12:00 (All Beijing Time)

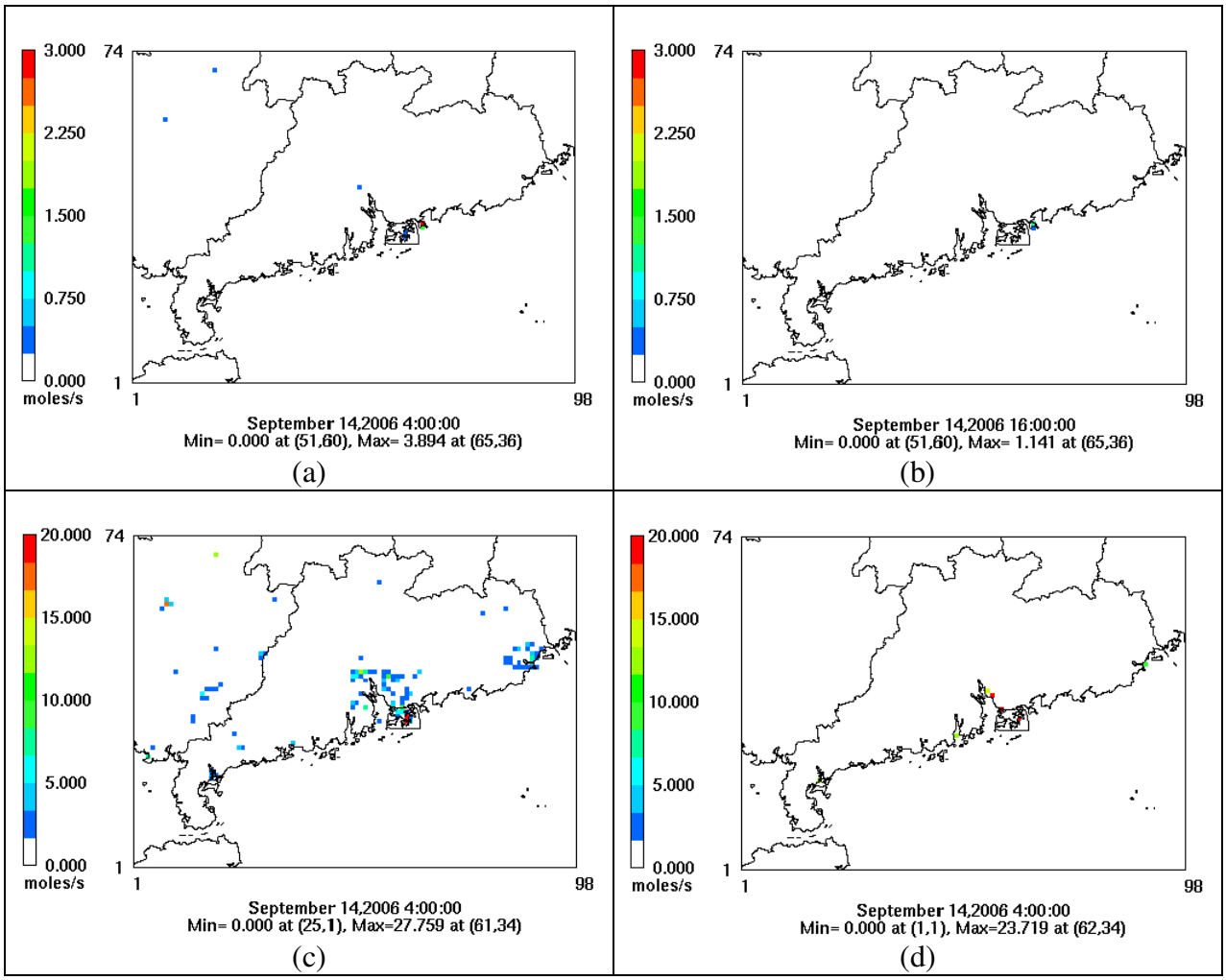

Figure 22 SO_2 emission in 9km × 9km domain 2: (a) layer 1 at 12:00; (b) layer 1 at 24:00; (c) layer 2 at 12:00; (d) layer 9 at 12:00 (All Beijing Time)

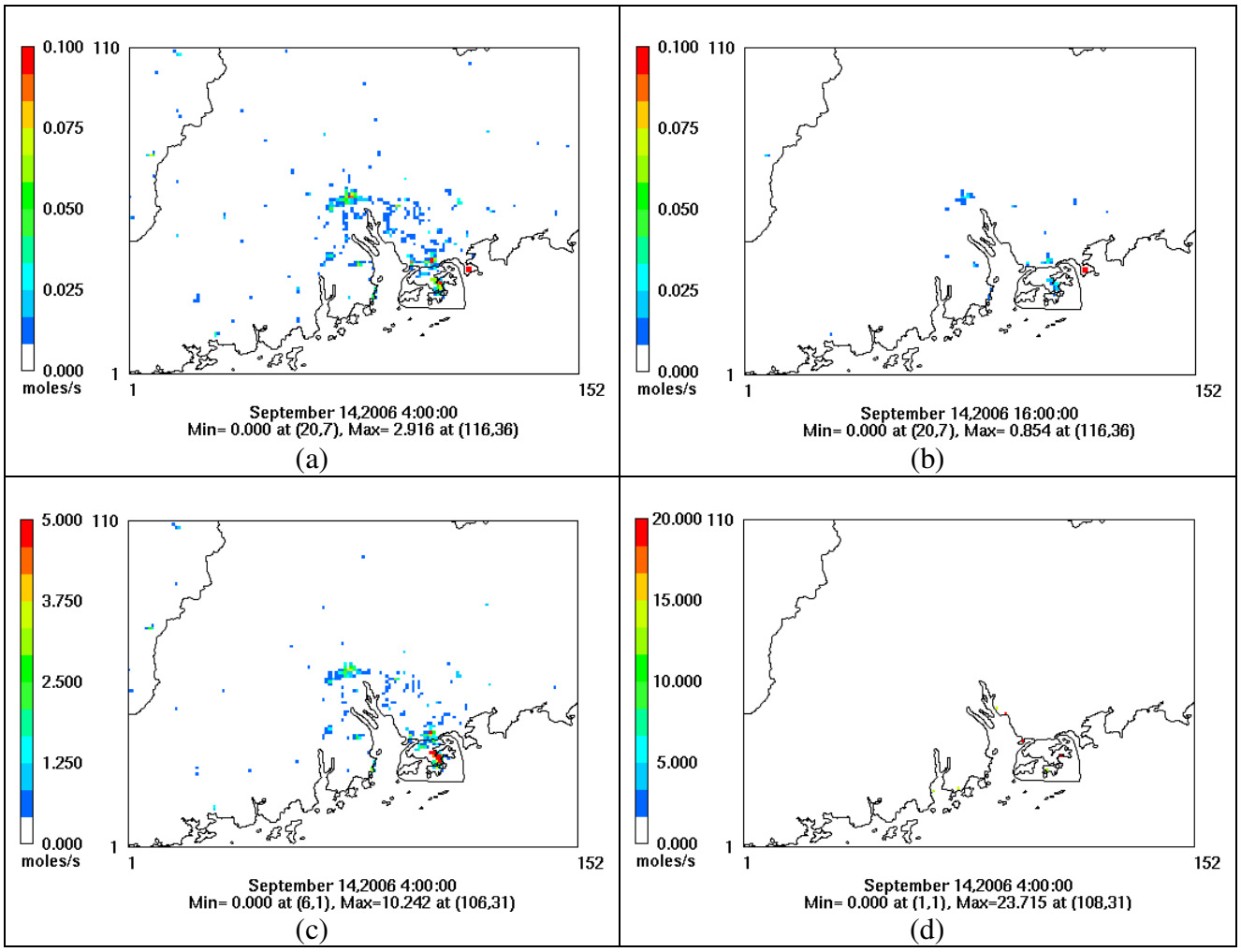

Figure 23 SO_2 emission in 3km × 3km domain 3: (a) layer 1 at 12:00; (b) layer 1 at 24:00; (c) layer 2 at 12:00; (d) layer 9 at 12:00 (All Beijing Time)

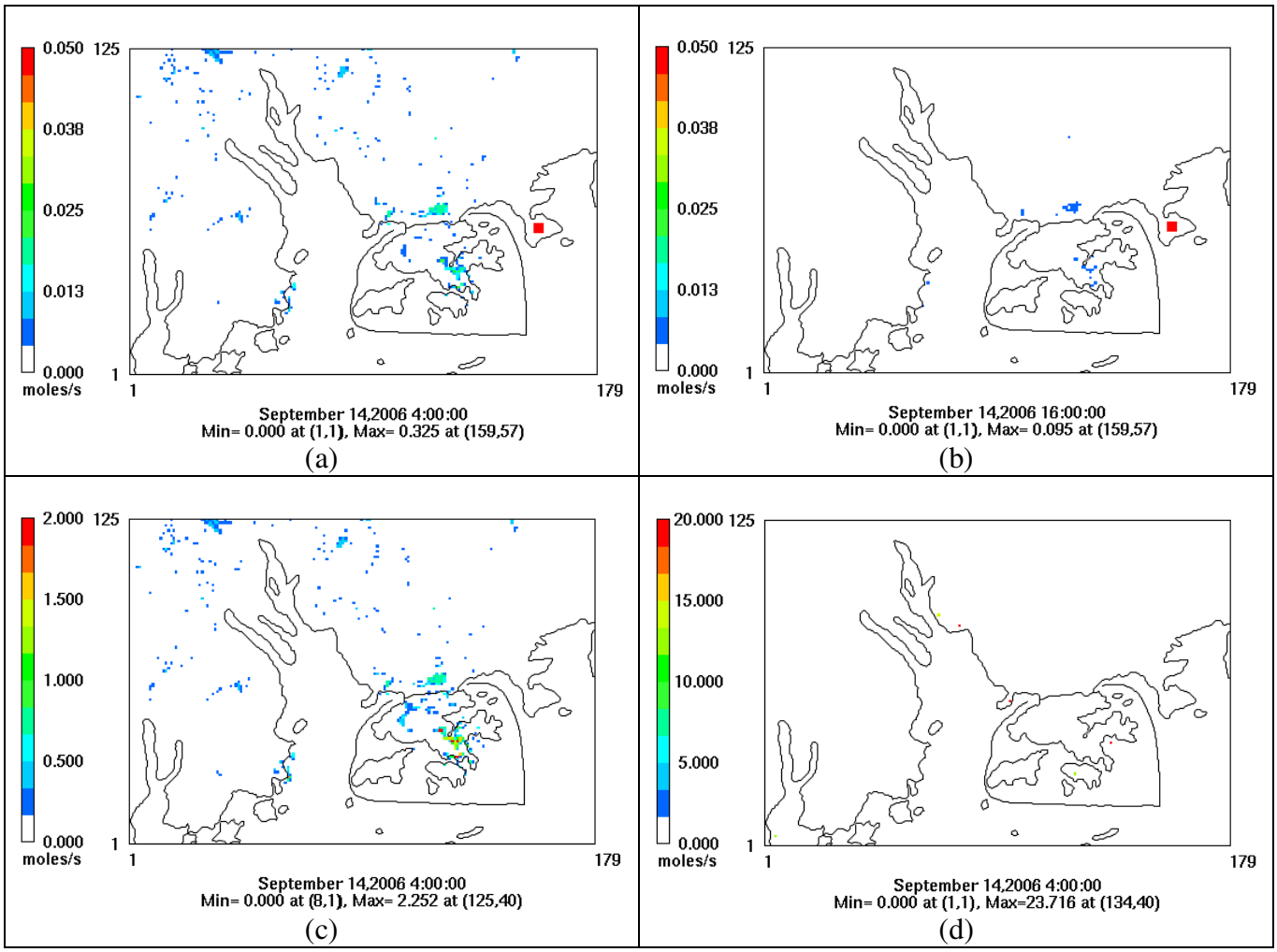

Figure 24 SO_2 emission in 1km × 1km domain 4: (a) layer 1 at 12:00; (b) layer 1 at 24:00; (c) layer 2 at 12:00; (d) layer 9 at 12:00 (All Beijing Time)

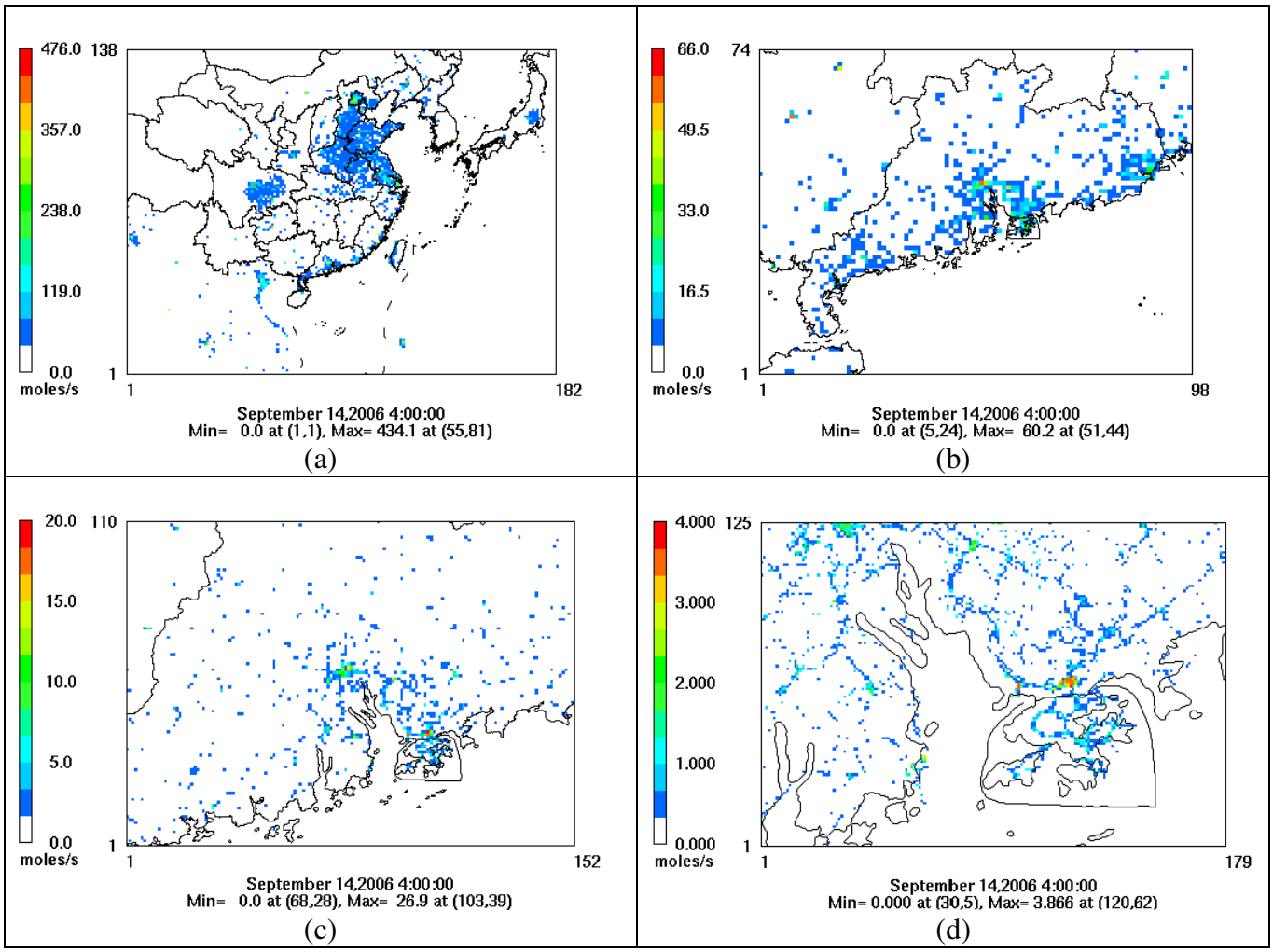

Figure 25 CO emission input at 12:00 (Beijing Time) in resolution of: (a) 27km × 27km; (b) 9km × 9km; (c) 3km × 3km; (d) 1km × 1km

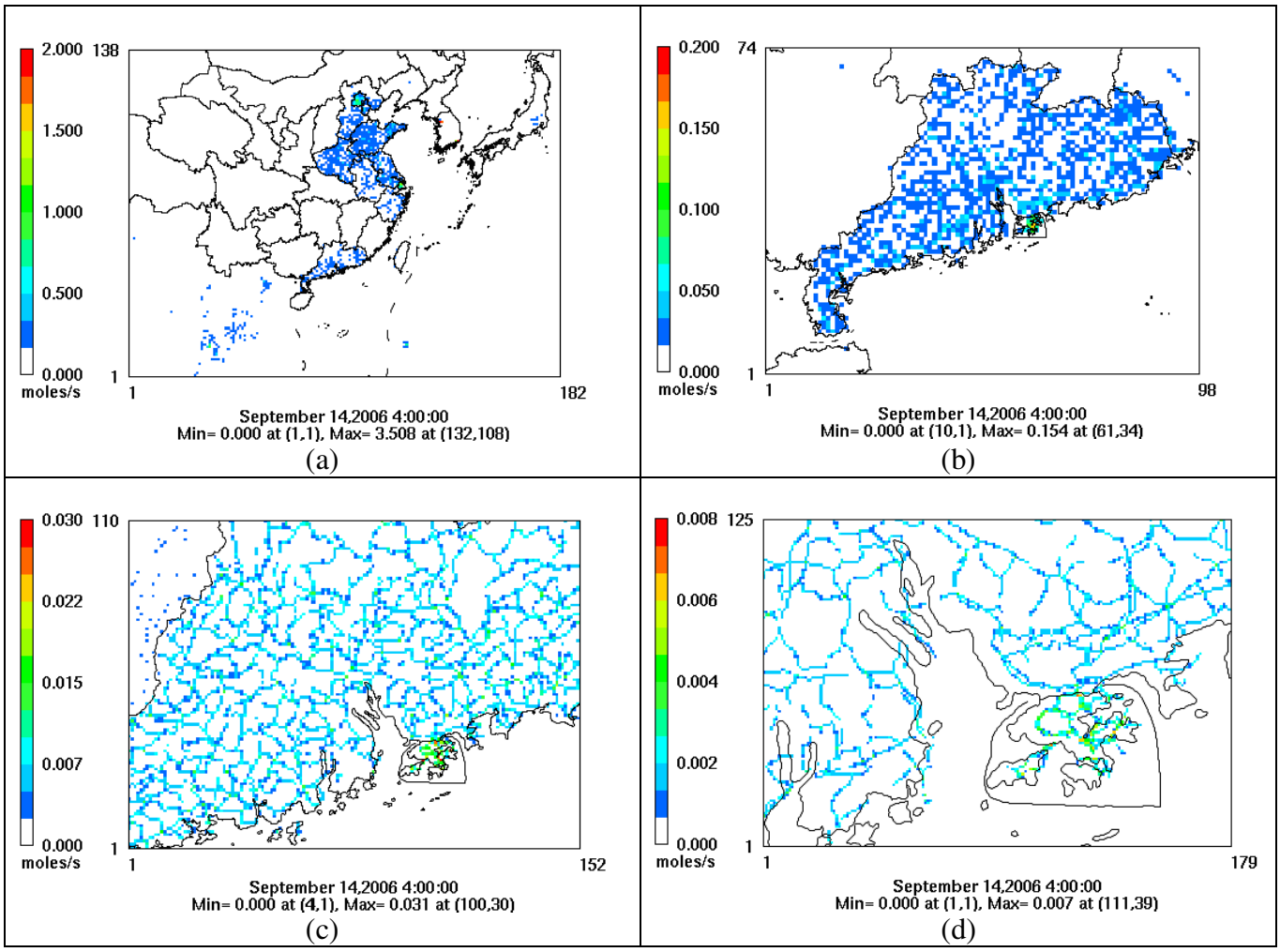

Figure 26 FORM emission input at 12:00 (Beijing Time) in resolution of: (a) 27km × 27km; (b) 9km × 9km; (c) 3km × 3km; (d) 1km × 1km

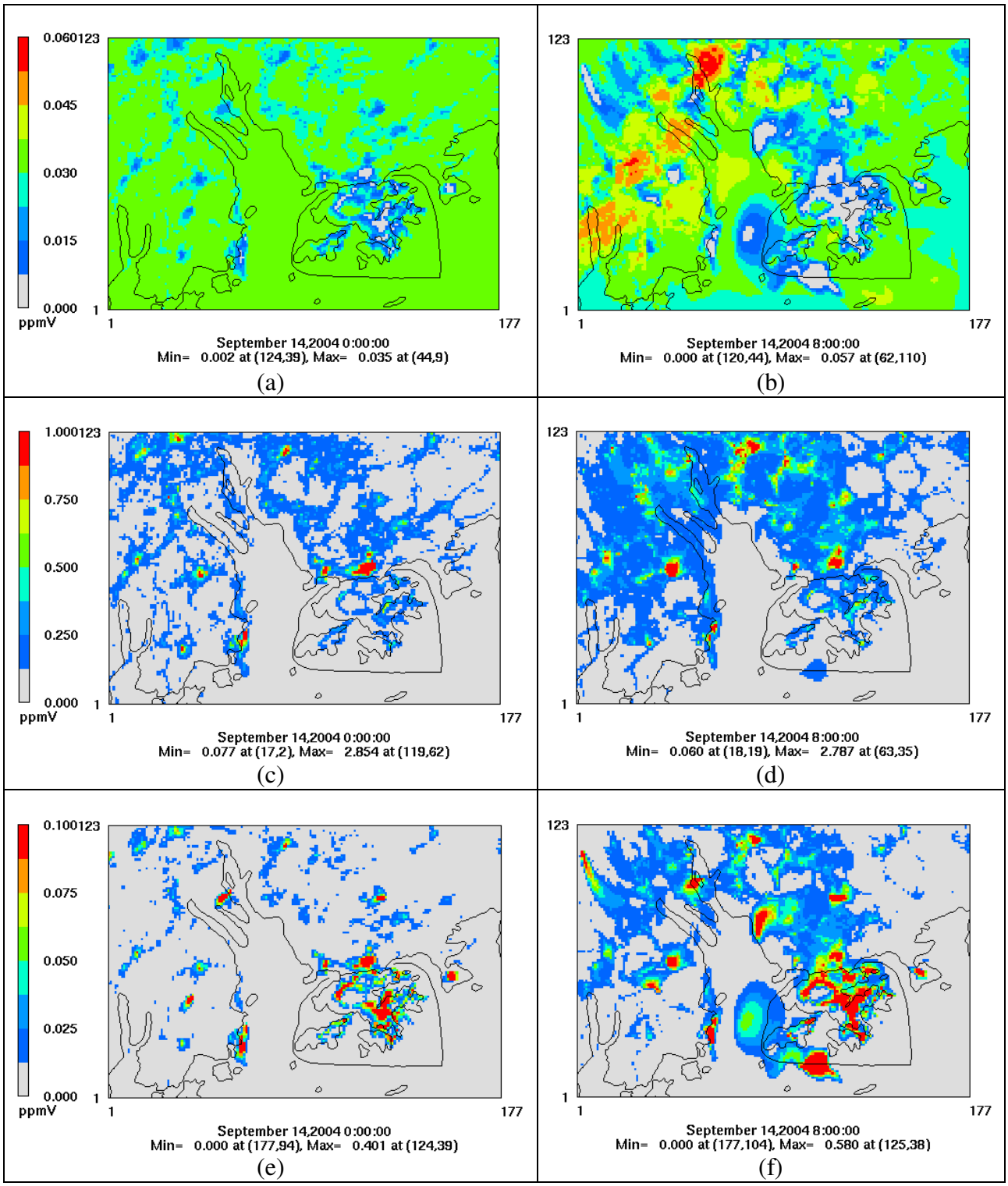

Figure 27 Preliminary results of CMAQ test run: (a): O_3 at 8:00; (b): O_3 at 16:00 (c): CO at 8:00; (d): CO at 16:00; (e): NOx at 8:00; (f): NOx at 16:00 (Beijing Time)

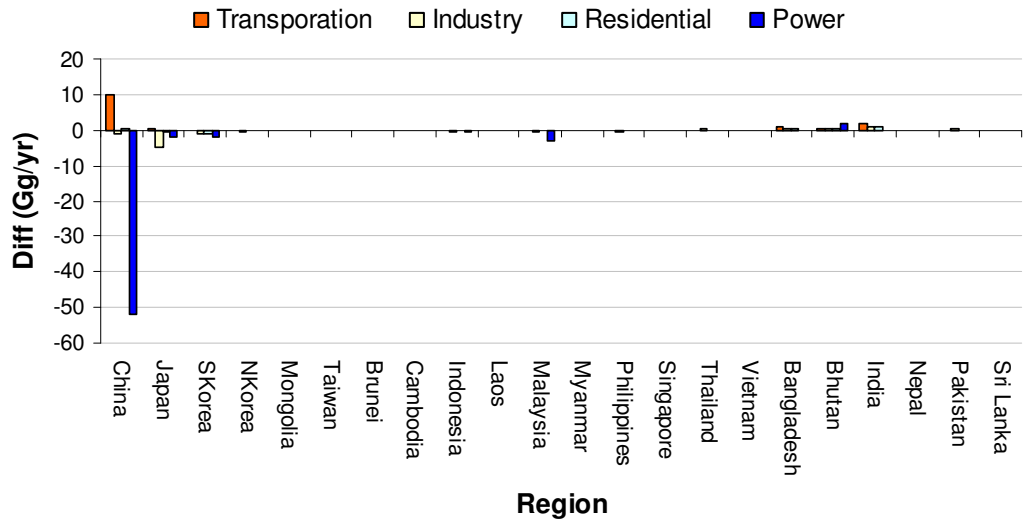

(a)

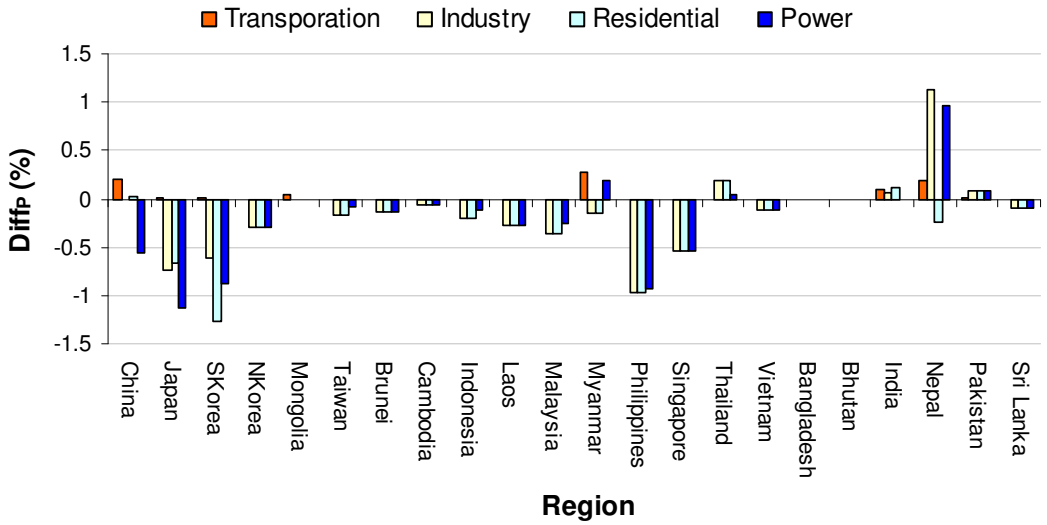

(b)

Figure 28 Sectoral difference percentages in resolution of 1km × 1km: (a) Difference; (b) Difference percentage

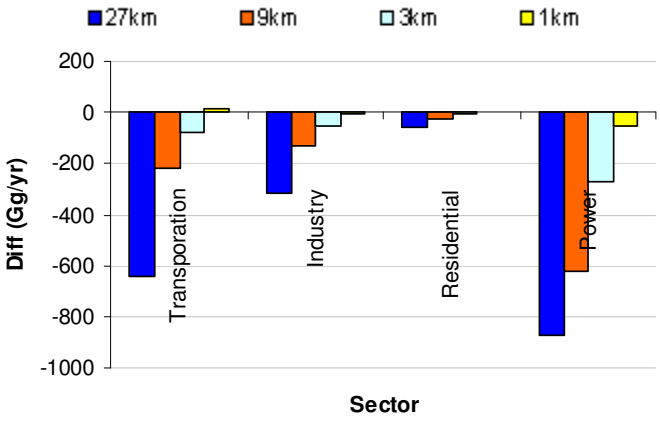

(a)

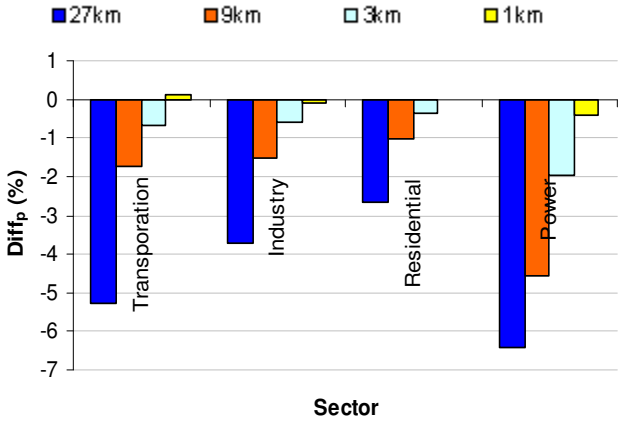

(b)

Figure 29 Comparison between ZonalSum and INTEX-B: (a) Difference; (b) Difference percentage

VITA

Yuan Du grew up in Sinan, a mountainous town in China. After receiving Bachelor's degree in Environmental Engineering from Tsinghua University, she decided to go to University of Tennessee for her master degree. During the two years in UT, she worked on air quality modeling with the specific concentration on Asian emission process. Now, She is planning to graduate this December and looking for a position in Air quality modeling area. She wants to be an expert in her major after five-year practical work.